



Combining livestock production information in a process-based vegetation model to reconstruct the history of grassland management

Jinfeng Chang^{1,2}, Philippe Ciais¹, Mario Herrero³, Petr Havlik⁴, Matteo Campioli⁵, Xianzhou Zhang⁶, Yongfei Bai⁷, Nicolas Viovy¹, Joanna Joiner⁸, Xuhui Wang^{9,10}, Shushi Peng¹⁰, Chao Yue^{1,11}, Shilong Piao¹⁰, Tao Wang^{12,13}, Didier A. Hauglustaine¹, Jean-Francois Soussana¹⁴, Anna Peregon^{1,15}, Natalya Kosykh¹⁵, and Nina Mironycheva-Tokareva¹⁵

¹Laboratoire des Sciences du Climat et de l'Environnement, UMR8212, CEA-CNRS-UVSQ, 91191 Gif-sur-Yvette, France

²Sorbonne Universités (UPMC), CNRS-IRD-MNH, LOCEAN/IPSL, 4 place Jussieu, 75005 Paris, France

³Commonwealth Scientific and Industrial Research Organisation, Agriculture Flagship, St. Lucia, QLD 4067, Australia

⁴Ecosystems Services and Management Program, International Institute for Applied Systems Analysis, 2361 Laxenburg, Austria

⁵Centre of Excellence PLECO (Plant and Vegetation Ecology), Department of Biology, University of Antwerp, 2610 Wilrijk, Belgium

⁶Lhasa Plateau Ecosystem Research Station, Key Laboratory of Ecosystem Network Observation and Modeling, Institute of Geographic Sciences and Natural Resources Research, CAS, 100101 Beijing, China

⁷State Key Laboratory of Vegetation and Environmental Change, Institute of Botany, Chinese Academy of Sciences, 100093 Beijing, China

⁸NASA Goddard Space Flight Center, Greenbelt, MD, USA

⁹Laboratoire de Météorologie Dynamique, Institute Pierre Simon Laplace, 75005 Paris, France

¹⁰Sino-French Institute of Earth System Sciences, College of Urban and Environmental Sciences, Peking University, 100871 Beijing, China

¹¹CNRS and UJF Grenoble 1, UMR5183, Laboratoire de Glaciologie et Géophysique de l'Environnement (LGGE), Grenoble, France

¹²Key Laboratory of Alpine Ecology and Biodiversity, Institute of Tibetan Plateau Research, Chinese Academy of Sciences, 100085 Beijing, China

¹³CAS Center for Excellence in Tibetan Plateau Earth Sciences, Chinese Academy of Sciences, 100085 Beijing, China

¹⁴INRA, UAR0233 CODIR Collège de Direction. Centre-Siège de l'INRA, Paris, France

¹⁵Institute of Soil Science and Agrochemistry, Siberian Branch Russian Academy of Sciences (SB RAS), Pr. Akademika Lavrentyeva 8/2, 630090 Novosibirsk, Russia

Correspondence to: Jinfeng Chang (jinfeng.chang@locean-ipsl.upmc.fr)

Received: 9 January 2016 – Published in Biogeosciences Discuss.: 18 February 2016

Revised: 26 May 2016 – Accepted: 8 June 2016 – Published: 29 June 2016

Abstract. Grassland management type (grazed or mown) and intensity (intensive or extensive) play a crucial role in the greenhouse gas balance and surface energy budget of this biome, both at field scale and at large spatial scale. However, global gridded historical information on grassland management intensity is not available. Combining modelled grass-biomass productivity with statistics of the grass-biomass demand by livestock, we reconstruct gridded maps of grassland management intensity from 1901 to 2012. These maps include the minimum area of managed vs. maximum area of unmanaged grasslands and the fraction of mown vs. grazed area at a resolution of 0.5° by 0.5° . The grass-biomass demand is derived from a livestock dataset for 2000, extended to cover the period 1901–2012. The grass-biomass supply (i.e. forage grass from mown grassland and biomass grazed) is simulated by the process-based model ORCHIDEE-GM driven by historical climate change, rising CO_2 concentration, and changes in nitrogen fertilization. The global area of managed grassland obtained in this study increases from $6.1 \times 10^6 \text{ km}^2$ in 1901 to $12.3 \times 10^6 \text{ km}^2$ in 2000, although the expansion pathway varies between different regions. ORCHIDEE-GM also simulated augmentation in global mean productivity and herbage-use efficiency over managed grassland during the 20th century, indicating a general intensification of grassland management at global scale but with regional differences. The gridded grassland management intensity maps are model dependent because they depend on modelled productivity. Thus specific attention was given to the evaluation of modelled productivity against a series of observations from site-level net primary productivity (NPP) measurements to two global satellite products of gross primary productivity (GPP) (MODIS-GPP and SIF data). Generally, ORCHIDEE-GM captures the spatial pattern, seasonal cycle, and interannual variability of grassland productivity at global scale well and thus is appropriate for global applications presented here.

1 Introduction

The rising concentrations of greenhouse gases (GHGs), such as carbon dioxide (CO_2), methane (CH_4), and nitrous oxide (N_2O), are driving climate change through increased radiative forcing (IPCC, 2013). It is estimated that, globally, livestock production (including crop-based and pasture-based) currently accounts for 37 and 65 % of the anthropogenic CH_4 and N_2O emissions respectively (Martin et al., 2010; FAO, 2006). Grassland ecosystems support most of the world's livestock production, thus contributing indirectly a significant share of global CH_4 and N_2O emissions. For CO_2 fluxes, however, grassland can be either a sink or a source with respect to the atmosphere. The annual changes in carbon storage of managed grassland ecosystems in Europe (hereafter referred to as net biome productivity, NBP) was found to

be correlated with carbon removed by grazing and/or mowing (Soussana et al., 2007). Thus, knowledge of management type (grazed or mown) and intensity (intensive or extensive) is crucial for simulating the carbon stocks and GHG fluxes of grasslands.

For European grasslands, Chang et al. (2015a) constructed management intensity maps over the period 1961–2010 based on (i) national-scale livestock numbers from statistics (FAOSTAT, 2014), (ii) static sub-continental grass-fed fractions for each animal type (Bouwman et al., 2005), and (iii) the grass-fed livestock numbers supported by the net primary productivity (NPP) of the ORCHIDEE-GM (ORGanizing Carbon and Hydrology In Dynamic Ecosystems grassland management) model. That study estimated an increasing NBP (i.e. acceleration of soil carbon accumulation) over the period 1991–2010. The increasing NBP was attributed to climate change, CO_2 trends, nitrogen (N) addition, and land-cover and management intensity changes. The observation-driven trends of management intensity were found to be the dominant driver explaining the positive trend of NBP across Europe (36–43 % of the total trend with all drivers; Chang et al., 2016). That study confirmed the importance of management intensity in drawing up a grassland carbon balance. However, the national-scale management intensity and the identical history maps between 1901 and 1960 in that study carried several sources of uncertainty (Chang et al., 2015a). It implies that long-term history of large-scale gridded information on grassland management intensity is needed. The HYDE 3.1 land-use dataset (Klein Goldewijk et al., 2011) provides reconstructed gridded changes of pasture area over the past 12 000 years. Here, “pasture” represents managed grassland providing grass biomass to livestock. This reconstruction is based on population density data and country-level per capita use of pasture land derived from FAO statistics (FAOSTAT, 2008) for the post-1961 period and assumed by those authors for the pre-1960 period. It defines land used as pasture but does not provide information about management intensity. To our knowledge, global maps of grassland management intensity history are not available.

Recently, Herrero et al. (2013) garnered global livestock data to create a dataset with gridded grass-biomass-use information for year 2000. In this dataset, grass used for grazing or silage is separated from grain feed, occasional feed, and stover (fibrous crop residues). A variety of constraints have been taken into account in creating this global dataset, including the specific metabolisable energy (ME) requirements for each animal species and regional differences in animal diet composition, feed quality, and feed availability. This grass-biomass-use dataset provides a starting point for constraining the amount of carbon removed by grazing and mowing (i.e. the target of grass-biomass use) and is suitable for adoption by global vegetation models to account for livestock-related fluxes.

The major objective of this study is to produce global gridded maps of grassland management intensity since 1901 for

global vegetation model applications. These maps combine historical NPP changes from the process-based global vegetation model ORCHIDEE-GM (Chang et al., 2013, 2015b) with gridded grass-biomass use extrapolated from Herrero et al. (2013). First, ORCHIDEE-GM is calibrated to simulate the distribution of “potential” (maximal) harvested and grazed biomass from mown and grazed grasslands respectively. In a second step, the modelled productivity maps are used in combination with livestock data to reconstruct annual maps of grassland management intensity, at a spatial resolution of 0.5° by 0.5° . This is done for each country since 1961 and for 18 large regions of the globe for 1901–1960. The reconstructed management intensity defines the fraction of mown, grazed, and unmanaged grasslands in each grid cell. The gridded grassland management intensity maps are model dependent because they rely on simulated NPP. Thus, in this study we also give a specific attention to the evaluation of modelled productivity against both a new set of site-level NPP measurements and satellite-based models of gross primary productivity (GPP). In Sect. 2, we describe the ORCHIDEE-GM model, the adjustment of its parameters for the C4 grassland biome, model input, the method proposed to reconstruct grassland management intensity, and the data used for evaluation. The derived management intensity maps and the comparison between modelled and observed productivity are presented in Sect. 3 and discussed in Sect. 4. Concluding remarks are made in Sect. 5.

2 Material and methods

2.1 Model description

ORCHIDEE is a process-based ecosystem model developed for simulating carbon fluxes, and water and energy fluxes in ecosystems, from site level to global scale (Krinner et al., 2005; Ciais et al., 2005; Piao et al., 2007). ORCHIDEE-GM (Chang et al., 2013) is a version of ORCHIDEE that includes the grassland management module from PaSim (Riedo et al., 1998; Vuichard et al., 2007a, b; Graux et al., 2011), a grassland model for field-level to continental-scale applications. Accounting for the management practices such as mowing, livestock grazing and organic fertilizer application on a daily basis, ORCHIDEE-GM proved capable of simulating the dynamics of leaf area index, biomass, and C fluxes of managed grasslands. ORCHIDEE-GM version 1 was evaluated and some of its parameters calibrated, at 11 European grassland sites representative of a range of management practices, with eddy-covariance net ecosystem exchange and biomass measurements. The model successfully simulated the NBP of these managed grasslands (Chang et al., 2013). Chang et al. (2015b) then added a parameterization of adaptive management through which farmers react to a climate-driven change of previous-year productivity. Though a full N cycle is not included in ORCHIDEE-GM, the positive

effect of nitrogen fertilizers on grass photosynthesis rates, and thus on subsequent ecosystem productivity and carbon storage, is parameterized with an empirical function calibrated from literature estimates (version 2.1; Chang et al., 2015b). ORCHIDEE-GM v2.1 was applied over Europe to calculate the spatial pattern, interannual variability (IAV), and the trends of potential productivity, i.e. the productivity that maximizes simulated livestock densities assuming an optimal management system in each grid cell (Chang et al., 2015b). This version was further used to simulate NBP and NBP trends over European grasslands during the last 5 decades at a spatial resolution of 25 km and a 30 min time step (Chang et al., 2015a).

ORCHIDEE-GM v1 and v2.1 were developed based on ORCHIDEE v1.9.6. To benefit from recent developments and bug corrections in the ORCHIDEE model, ORCHIDEE-GM is updated in this study with ORCHIDEE Trunk.rev2425 (available at <https://forge.ipsl.jussieu.fr/orchidee/browser/trunk#ORCHIDEE>). We further made the adjustment of its parameters for the C4 grassland biome (Sect. 2.2) and implemented a specific strategy for wild herbivores grazing (Sect. 2.3; also see Supplement Sect. S1). The updated model is referred to hereafter as ORCHIDEE-GM v3.1.

2.2 Model parameter settings

ORCHIDEE-GM was applied to simulate GHG budgets and ecosystem carbon stocks under climate, CO_2 , and management changes for Europe. However, an extension of model application to regions outside Europe requires first a calibration of key productivity-related parameters. Two sensitive parameters representing photosynthetic capacity (the maximum rate of Rubisco carboxylase activity at a reference temperature of 25°C ; $V_{c_{\max}25}$) and the morphological plant traits (the maximum specific leaf area; SLA_{\max}) were reported by Chang et al. (2015a) for simulating grassland NPP. The $V_{c_{\max}25} = 55 \mu\text{mol m}^{-2} \text{s}^{-1}$ and $\text{SLA}_{\max} = 0.048 \text{ m}^2 \text{ per g C}$ in ORCHIDEE-GM were previously defined from observations and indirectly evaluated against eddy-flux tower measurements of GPP for temperate C3 grasslands in Europe (Chang et al., 2013, 2015b). The global TRY database gives SLA values for C4 grasses, of $0.0192 \text{ m}^2 \text{ g}^{-1}$ dry matter (DM) ($0.0403 \text{ m}^2 \text{ per g C}$ with a mean leaf carbon content per DM of 47.61%; Kattge et al., 2011). Thus, we have set the value of $\text{SLA}_{\max} = 0.044 \text{ m}^2 \text{ per g C}$ for C4 grasses in ORCHIDEE-GM to fit the mean value from the TRY estimate, as we did previously for C3 grasses (Chang et al., 2013). The parameter $V_{c_{\max}25}$ cannot be directly measured, but it is usually derived from A/C_i curves in C3 or C4 photosynthesis models (C3: Farquhar et al., 1980; C4: Collatz et al., 1992), where A is the leaf-scale net CO_2 assimilation rate and C_i the partial pressure of CO_2 in leaf intercellular spaces. Several researches provide observation-based estimates of $V_{c_{\max}25}$ (Feng and Dietze, 2013; Verheijen et al., 2013; range of $24\text{--}131 \mu\text{mol m}^{-2} \text{s}^{-1}$ for C3 grasses and

of 15–46 $\mu\text{mol m}^{-2} \text{s}^{-1}$ for C4 grasses). Based on these estimates, we keep the value of $V_{\text{c}_{\text{max}}25} = 55 \mu\text{mol m}^{-2} \text{s}^{-1}$ previously calibrated in Europe for all C3 grasses and set $V_{\text{c}_{\text{max}}25} = 25 \mu\text{mol m}^{-2} \text{s}^{-1}$ for C4 grasses. These values may reflect neither differences in nitrogen and phosphorus availability between locations nor adaptation or species changes within a C3 or C4 grassland, but they are within the range of observations made under different conditions and consistent with values used by other terrestrial ecosystem models (Table S1 in the Supplement). All other parameters of ORCHIDEE model are kept the same as in Trunk.rev2425. The parameter settings for grassland management module are in consistent with that in ORCHIDEE-GM v1 (Chang et al., 2013) and v2.1 (Chang et al., 2015a, b).

2.3 Model input

ORCHIDEE-GM v3.1 was run on a global grid over the globe using the 6-hourly CRU+NCEP reconstructed climate data at $0.5^\circ \times 0.5^\circ$ spatial resolution for the period 1901–2012 (Viovy, 2013). The fields used as input of the model are temperature, precipitation, specific humidity, solar radiation, wind speed, pressure, and long-wave radiation. Other input data are (1) yearly domestic grazing-ruminant stocking density maps, (2) wild-herbivores population density maps, (3) N fertilizer application maps including manure-N and mineral-N fertilizers, and (4) atmospheric-N deposition maps. These input maps all cover the period from 1901 to 2012 and are briefly described below (also see Supplement Sects. S2–S5). Table 1 lists all variables shown in this section, including their abbreviations, units, related equations, and data sources.

Grazing-ruminant stocking density maps: spatial statistical information on grazing-ruminant stocking density is not available at global scale. In this study, we combined the domestic ruminant stocking density maps (Supplement Sect. S2) and historic land-cover change maps (Supplement Sect. S3) to construct gridded grazing-ruminant stocking density.

Assuming that all the ruminants in each grid cell were grazing on the grassland within the same grid, we defined the grazing-ruminant stocking density in grid cell k in year m ($D_{\text{grazing},m,k}$, livestock unit (LU) per ha of grassland area) as

$$D_{\text{grazing},m,k} = \frac{D_{m,k}}{f_{\text{grass},m,k}}, \quad (1)$$

where $D_{m,k}$ is the total domestic ruminant stocking density (unit: LU per ha of land area; Supplement Sect. S2) and $f_{\text{grass},m,k}$ is the grassland fraction in grid cell k in year m from a set of historic land-cover-change maps (Supplement Sect. S3). To avoid unrealistic densities of ruminant grazing over grassland (which might cause grasses to die during the growing season), a maximum value of 5 LU ha⁻¹ was set for the density map. In addition, a minimum grazing-ruminant

density of 0.2 LU ha⁻¹ was set to avoid economically implausible stocking rates. Figure S1 in the Supplement shows the example maps of domestic ruminant stocking density (D) and the corresponding grazing-ruminant stocking density (D_{grazing}) for reference year 2006.

Wild herbivore density maps: gridded maps of wild herbivore density are not available; therefore the gridded population density of wild herbivores (D_{wild} ; unit: LU per ha of grassland area) is derived from the literature data and from Bouwman et al. (1997) (see Table S2 for detail). The population of these herbivores from literature was first converted to LU according to the ME requirement calculated from their mean weight (Table S2) and then distributed to suitable grasslands based on grassland aboveground (consumable) NPP simulated from ORCHIDEE-GM v3.1 (Supplement Sect. S4; Fig. S2). The wild herbivores density was assumed to remain constant during the period of 1901–2012, because no worldwide historical wild-animal population information was available. A specific grazing strategy for wild herbivores is incorporated in the model (Supplement Sect. S1). We assumed wild herbivores eat fresh grass biomass during the growing season and eat dead grass during the non-growing season.

Nitrogen application rates from mineral fertilizers and manure: grassland is fertilized with organic N fertilizer (e.g. manure, slurry) and/or even mineral-N fertilizer, though this is not as common as for cropland. Gridded fertilizer application rates on grassland are not available worldwide. The only exception that we are aware of is for European grasslands (Leip et al., 2008, 2011, 2014; data available for EU-27 as used in Chang et al., 2015a). For countries/regions other than EU-27, the following data were used. The amount of manure-N fertilizer for 17 world regions at 1995 was derived from various sources (e.g. IFA, 1999; FAO/IFA/IFDC, 1999; FAO/IFA, 2001) and synthesized by Bouwman et al. (2002a, b; Table S3). For mineral-N fertilizers on grassland, country-scale data of fertilized area and mean fertilization rate for 1999/2000 are available in FAO/IFA/IFDC/IPI/PPI (2002) with grassland/pasture been fertilized in 13 non-EU countries. The regional/country-scale data were downscaled to a $0.5^\circ \times 0.5^\circ$ grid and extended to cover the period 1901–2012 (see Supplement Sect. S5 for detail).

Atmospheric-nitrogen deposition maps: the historical atmospheric-N deposition maps were simulated by the LMDz-INCA-ORCHIDEE global chemistry–aerosol–climate model (Hauglustaine et al., 2014). Hindcast simulations for the years 1850, 1960, 1970, 1980, 1990, and 2000 have been performed using anthropogenic emissions from Lamarque et al. (2010). The total nitrogen deposition fields (wet and dry; NH_x and NO_y) of all nitrogen-containing gas-phase and aerosol species have been simulated at a spatial resolution of 1.9° in latitude and 3.75° in longitude. Linear interpolation was performed between the hindcast snapshot years to produce temporally variable

Table 1. The abbreviations, units, related equations, and data sources of the variables shown in this study.

Abbreviations ^a	Variables	Units ^b	Related equations	Sources
D	Domestic ruminant stocking density	LU per ha of land area	Eqs. (1), (2), (S3), (S4), (S5)	Robinson et al. (2014); FAOSTAT, 2014
D_{grazing}	Grazing-ruminant stocking density	LU ha ⁻¹	Eqs. (1), (3)	Robinson et al. (2014); FAOSTAT (2014); Bartholomé and Belward (2005); Eva et al. (2004); Poulter et al. (2011); Hurtt et al. (2011)
D_{wild}	Wild herbivore density	LU ha ⁻¹	Eq. (S6)	Synthesized by Bouwman et al. (1997)
N_{manure}	Organic (manure) nitrogen fertilizer application rate	kg N ha ⁻¹ yr ⁻¹	Eqs. (S7), (S8)	Synthesized by Bouwman et al. (2002a, b)
N_{mineral}	Mineral-nitrogen fertilizer application rate	kg N ha ⁻¹ yr ⁻¹	Eq. (S9)	FAO/IFA/IFDC/IPI/PPI (2002)
$N_{\text{deposition}}$	Atmospheric-nitrogen deposition rate	kg N ha ⁻¹ yr ⁻¹		Hauglustaine et al. (2014)
GBU	Grass-biomass use	kg DM yr ⁻¹	Eqs. (2), (4), (7)	Herrero et al. (2013); FAOSTAT (2014)
Y_{mown}	Annual potential harvested biomass from mown grasslands	kg DM m ⁻² yr ⁻¹	Eqs. (7), (10), (11)	this study
Y_{graze}	Annual potential biomass consumption over grazed grasslands	kg DM m ⁻² yr ⁻¹	Eqs. (3), (4), (7), (10), (11)	this study
A_{grass}	Grassland area	m ²	Eqs. (4), (7)	Bartholomé and Belward (2005); Eva et al. (2004); Poulter et al. (2011); Hurtt et al. (2011)
f_{grass}	Grassland fraction	Percent (%)	Eq. (1)	Bartholomé and Belward (2005); Eva et al. (2004); Poulter et al. (2011); Hurtt et al. (2011)
f_{mown}	Minimum fraction of mown grassland	Percent (%)	Eqs. (5), (7), (8), (10), (11)	this study
f_{grazed}	Minimum fraction of grazed grassland	Percent (%)	Eqs. (4), (6), (7), (8), (10), (11)	this study
$f_{\text{unmanaged}}$	Maximum fraction of unmanaged grassland	Percent (%)	Eqs. (6), (9), (10), (11)	this study

^a The subscripts of these variables in this study: i is ruminant category; j is country; k is grid cell; m is year; q is region.

^b When not specified, the ha⁻¹ (or m⁻²) in the units indicate per ha (or per m²) of grassland area.

atmospheric-N deposition maps ($N_{\text{deposition}}$, unit: kg N per ha of grassland area per year).

2.4 Simulation set-up

Considering different photosynthetic pathways and management types, six grassland plant functional types (PFTs) are defined: C3 natural (unmanaged) grassland, C3 mown grass-

land, C3 grazed grassland, C4 natural (unmanaged) grassland, C4 mown grassland, and C4 grazed grassland. In the simulation, we ideally consider that grassland PFTs are distributed all over the world. Post-processing will incorporate the information of grassland distribution in the real world (Supplement Sect. S3). ORCHIDEE-GM v3.1 is run over the globe during the period 1901–2012, forced by increasing CO₂, variable climate, and variable nitrogen deposition

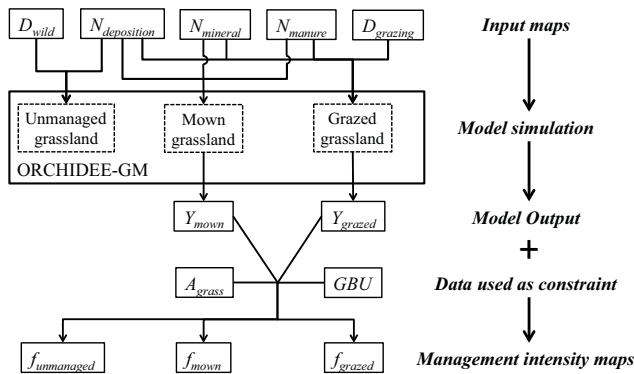


Figure 1. Illustration of the procedures for reconstructing management intensity maps. Italic texts indicate the major steps of the reconstruction. The meanings, units, related equations, and data sources of the variables (i.e. gridded maps) are shown in Table 1. D_{grazing} is grazing-ruminant stocking density; D_{wild} is wild herbivore density; N_{manure} is organic (manure) nitrogen fertilizer application rate; N_{mineral} is mineral-nitrogen fertilizer application rate; $N_{\text{deposition}}$ is atmospheric-nitrogen deposition rate; Y_{mown} is annual potential harvested biomass from mown grasslands; Y_{grazed} is annual potential grazed biomass from grazed grasslands; GBU is grass-biomass use; f_{mown} is minimum fraction of mown grassland; f_{grazed} is minimum fraction of grazed grassland; $f_{\text{unmanaged}}$ is maximum fraction of unmanaged grassland.

($N_{\text{deposition}}$). For each grassland PFT, specific forcing and management strategies are used (summarized in Fig. 1). Unmanaged grasslands are forced by wild herbivore density maps (D_{wild}). Both mown and grazed grasslands are forced by the historical N fertilizer maps described above, which include manure (N_{manure}) and mineral fertilizers (N_{mineral}). Grazed grassland is additionally forced by the historical gridded grazing-ruminant stocking density (D_{grazing}).

2.5 Grassland management intensity and historical changes

Figure 1 briefly illustrates the procedures of combining model output, grass-biomass-use data, and grassland area data to reconstruct grassland management intensity maps. This section presents the procedures of the reconstruction in detail. Table 1 lists all variables shown in this section, including their abbreviations, units, related equations, and data sources.

Herrero et al. (2013) established a global livestock production dataset containing a high-resolution (8 km × 8 km) gridded map of grass-biomass use for the year 2000. In this study, this dataset is extrapolated annually over 1901–2012 to constrain the grass-biomass consumption in ORCHIDEE-GM v3.1. Assuming that grass-biomass use for grid cell k in country j and year m ($GBU_{m,j,k}$, unit: kg DM per year) varies proportionally with the total ME requirement of domestic ruminants in each country, $GBU_{m,j,k}$ can be calculated from its value of the year 2000 given by Herrero et

al. (2013), according to

$$GBU_{m,k} = GBU_{2000,k} \times \frac{D_{m,k}}{D_{2000,k}}, \quad (2)$$

where $D_{m,k}$ and $D_{2000,k}$ are the total ruminant stocking density for grid cell k in year m and in year 2000 calculated by Eqs. (S4) and (S5) in Supplement Sect. S2, which take into account the changes in category-specific ME requirement at country scale (1961–2012) or regional scale (1901–1960).

ORCHIDEE-GM v3.1 simulates the annual potential (maximal) harvested biomass from mown grasslands (Y_{mown} , unit: kg DM m⁻² yr⁻¹ from mown grassland) and the annual potential biomass consumption per unit area of grazed grassland (Y_{grazed} , unit: kg DM m⁻² yr⁻¹ from grazed grassland) in each grid cell. Under mowing, the frequency and magnitude of forage harvests in each grid cell is a function of grown biomass (Vuichard et al., 2007a). The effective yield on grazed grassland (i.e. Y_{grazed}) depends on the grazing stocking rate (here, D_{grazing}) and on the environmental conditions of the grid cell (Chang et al., 2015a); it is calculated as

$$Y_{\text{grazed},m,k} = IC \times T_{\text{grazing},m,k} \times D_{\text{grazing},m,k}, \quad (3)$$

where IC is the daily intake capacity for 1 LU (~ 18 kg DM per day calculated in Supplement Sect. S1 of Chang et al., 2015b), and $T_{\text{grazing},m,k}$ is the number of grazing days in grid cell k at year m . Due to the impact of livestock on grass growth through trampling, defoliation (i.e. biomass intake), etc., and because grassland cannot be continuously grazed during the vegetation period, thresholds of shoot biomass are set for starting, stopping, and resuming grazing (Vuichard et al., 2007a). The “recovery” time required under grazing is obtained in the model using threshold (Vuichard et al., 2007a; Chang et al., 2015a), which determines when grazing stops (dry biomass remaining lower than 300 kg DM ha⁻¹) or when grazing can start again (dry biomass recovered to a value above 300 kg DM ha⁻¹ for at least 15 days). Y_{grazed} is usually lower than Y_{mown} in temperate grasslands due to the lower herbage-use efficiency of grazing simulated by ORCHIDEE-GM (Chang et al., 2015b). However, in some arid regions the grass biomass does not grow enough during the season to trigger harvest; i.e. it does not reach the threshold in the model at which farmers are assumed to decide to cut grass for feeding forage to animals (see Chang et al., 2015b), so that Y_{grazed} can become larger than Y_{mown} (Fig. S3). The following set of rules was used to reconstruct historical changes in grassland management intensity, based on NPP simulated by ORCHIDEE-GM v3.1.

- Rule 1: for each grid cell and year, the total biomass removed by either grazing and cutting must be equal to the grass-biomass use, $GBU_{m,k}$.
- Rule 2: grazing management prioritizes in fulfilling $GBU_{m,k}$.

- Rule 3: if the potential biomass consumption from grazing (Y_{grazed}) is not high enough to fulfil $\text{GBU}_{m,j,k}$, a combination of grazing and mowing management is taken.

Thus, for grid cell k in year m , the minimum fraction of grazed ($f_{\text{grazed},m,k}$), the minimum fraction of mown ($f_{\text{mown},m,k}$), and the maximum fraction of unmanaged grassland ($f_{\text{unmanaged},m,k}$) are calculated with the following equations (definitions of minimum and maximum in this context are given below).

If $A_{\text{grass},m,k} \times Y_{\text{grazed},m,k} > \text{GBU}_{m,k}$, then

$$f_{\text{grazed},m,k} = \frac{\text{GBU}_{m,k}}{A_{\text{grass},m,k} \times Y_{\text{grazed},m,k}} \quad (4)$$

$$f_{\text{mown},m,k} = 0 \quad (5)$$

$$f_{\text{unmanaged},m,k} = 1 - f_{\text{grazed},m,k}, \quad (6)$$

where $A_{\text{grass},m,k}$ (unit: m^2) is the grassland area for grid cell k in year m of the series of historic land-cover change maps (Supplement Sect. S3).

If $A_{\text{grass},m,k} \times Y_{\text{grazed},m,k} < \text{GBU}_{m,k}$ and $A_{\text{grass},m,k} \times Y_{\text{mown},m,k} > \text{GBU}_{m,k}$ then

$$f_{\text{grazed},m,k} \times A_{\text{grass},m,k} \times Y_{\text{grazed},m,k} + f_{\text{mown},m,k} \times A_{\text{grass},m,k} \times Y_{\text{mown},m,k} = \text{GBU}_{m,k} \quad (7)$$

$$f_{\text{grazed},m,k} + f_{\text{mown},m,k} = 1 \quad (8)$$

$$f_{\text{unmanaged},m,k} = 0. \quad (9)$$

If $\text{GBU}_{m,k}$ cannot be fulfilled by any combination of modelled Y_{grazed} and Y_{mown} , we diagnose a modelled grass-biomass production deficit and apply the following equations:

$$\text{if } Y_{\text{grazed}} > Y_{\text{mown}}, \text{ then } f_{\text{grazed},m,k} = 1, f_{\text{mown},m,k} = 0, \text{ and } f_{\text{unmanaged},m,k} = 0, \quad (10)$$

$$\text{if } Y_{\text{grazed}} < Y_{\text{mown}}, \text{ then } f_{\text{mown},m,k} = 1, f_{\text{grazed},m,k} = 0, \text{ and } f_{\text{unmanaged},m,k} = 0. \quad (11)$$

This set of equations is valid for a mosaic of different types of grasslands in each grid cell, some managed (grazed and/or mown) and some remaining unmanaged. In reality, (1) farm owners could increase the mown fraction to produce more forage, which corresponds approximately to the mixed and landless systems of Bouwman et al. (2005); and (2) animals could migrate a long way across grazed and unmanaged fractions (as they do in real rangelands) and only select the most digestible grass in pastoral systems, which corresponds to extensively grazed grasslands. Yet, given the approximations made in this study, $f_{\text{grazed},m,k}$ and $f_{\text{mown},m,k}$ represent the minimum fractions of grazed/mown grasslands rather than the actual fractions, and $f_{\text{unmanaged},m,k}$ corresponds to a maximum fraction of unmanaged grasslands since both mixed and landless and extensive grazing are not modelled.

Herbage-use efficiency (Hodgson, 1979) is defined as the forage removed expressed as a proportion of herbage growth. It can be an indicator of management intensity over managed grassland, in addition to the fraction of managed area obtained above. In this study, the forage removed is modelled annual grass-biomass use including Y_{grazed} and Y_{mown} , and herbage growth is modelled annual grass GPP.

2.6 Model evaluation: datasets and model–data agreement metrics

The gridded grassland management intensity maps are model dependent because they depend on modelled productivity. Thus the evaluation of modelled productivity becomes necessary. In this study, modelled productivity (NPP and GPP) is compared to a new set of site-level NPP measurements (Sect. 2.7.1) and two satellite-based models of GPP (MODIS-GPP, from the Moderate Resolution Imaging Spectroradiometer, Sect. 2.7.2; sun-induced chlorophyll fluorescence (SIF) data, Sect. 2.7.3). Modelled NPP (or GPP) combines grassland productivity of all PFTs (Sect. 2.4), accounting for the variable fractions of grazed, mown, and unmanaged grassland in each grid cell calculated by Eqs. (4–11), and hereafter is referred to as $\text{NPP}_{\text{model}}$ (or $\text{GPP}_{\text{model}}$). Model–data agreement of NPP and GPP was assessed using Pearson’s product-moment correlation coefficients (r) and root mean squared errors (RMSEs).

2.6.1 Grassland NPP observation database

NPP is a crucial variable in vegetation models and it is essential that this variable is properly validated. High-quality measurements of grassland NPP are scarce, partly due to the difficulty of measuring some NPP components such as fine-root production (Scurlock et al., 1999, 2002). An updated version of the Luyssaert et al. (2007) database comprising non-forest biomes (Campioli et al., 2015) was used here. This database contains a flag indicating managed or unmanaged to each site and provides mean annual temperature, annual precipitation, and downwelling solar radiation based on site measurements from the literature, CRU database (Mitchell and Jones, 2005), MARS database (<http://mars.jrc.ec.europa.eu/mars/About-us/AGRI4CAST/Data-distribution/AGRI4CAST-Interpolated-Meteorological-Data>), or WorldClim database (Hijmans et al., 2005). Three additional datasets used in this study present NPP measurements from 30 sites across China (Zeng et al., 2015; Y. Bai, personal communication, 2015) and 16 sites across western Siberia (Peregon et al., 2008; with data updated to 2012). Data from China include NPP observations at fenced (i.e. unmanaged) and unfenced (i.e. managed) grassland for each site, and data of western Siberia are observations from natural wetland. In total, we have 305 NPP observations (NPP_{obs}) with separated aboveground and belowground NPP from 129 sites all over the world (including grassland, wetland, and

savanna; Fig. S4). Duplicate observations from the same site year were averaged and considered as a single entry. NPP measurements with different management (managed or unmanaged) at the same site were considered as identical observations. In total, 270 grassland NPP measurements were compared to the simulation of ORCHIDEE-GM v3.1 for the grid cell, corresponding to each site and for the time period of observation. Depending on the status of measured grassland (unmanaged or managed), modelled NPP from unmanaged or managed grassland is used for comparison. Modelled NPP over managed grassland accounts for the NPP from mown and grazed grassland and their corresponding fractions.

2.6.2 Grassland GPP from MODIS products

The MOD17A3 dataset (version 55; Zhao et al., 2005; Zhao and Running, 2010) – a MODIS product on vegetation production – provides the seasonal and annual GPP data at a spatial resolution of 1 km from 2000 to 2013. To obtain the grassland GPP from the MOD17 dataset, we first extract the MOD17 GPP at 1 km resolution over grassland grids in the MOD12Q1 dataset. Here, the grassland in the MOD12Q1 dataset includes the “open shrubland”, “savanna”, and “grassland” in the Boston University’s UMD classification scheme. The extracted annual and seasonal MODIS GPP was then averaged and aggregated to $0.5^\circ \times 0.5^\circ$ spatial resolution to be comparable to model output.

2.6.3 Sun-induced chlorophyll fluorescence data

Space-based observations of SIF provide a time-resolved measurement of a proxy of photosynthesis (Guanter et al., 2014). Similar to the MPI-BGC data-driven GPP product (Jung et al., 2011), SIF values exhibit a linear relationship ($r^2 = 0.79$) with monthly tower GPP at grassland sites in western Europe (Guanter et al., 2014). Compared to MODIS EVI (MOD13C2 products), SIF observations drop to zero during the non-growing season, thus providing a clearer signal of photosynthetic activity (Guanter et al., 2014) than other vegetation indices based on visible and near-infrared reflectances. SIF also provides a better seasonal agreement with GPP from flux towers as compared to vegetation indices (Joiner et al., 2014).

In this study, we used monthly GOME-2 (version 26, level 3) SIF data products with the spatial resolution of $0.5^\circ \times 0.5^\circ$ (available from 2007 to 2012). SIF-GPP is calculated by a SIF-GPP linear model adjusted from Guanter et al. (2014) ($\text{SIF-GPP} = -0.1 + 4.65 \times \text{SIF}$ (V26); see Supplement Sect. S6 for detail). To reduce the contamination of SIF by non-grassland PFTs, we restrict the model–data comparison to grassland-dominated grid cells, defined as those with grassland cover in the MOD12Q1 dataset (Sect. 2.5.2) is larger than 50 %.

3 Results

3.1 Maps of grassland management intensity

Figure 2 shows the minimum fractions of mown and grazed grasslands and the maximum fraction of unmanaged out of total grassland (f_{mown} , f_{grazed} , and $f_{\text{unmanaged}}$ respectively; Sect. 2.4) in the year 2000. Grazed grasslands comprise most of the managed grasslands in the maps (Fig. 2b). Significant fractions of mown grasslands are only found in regions with high ruminant stocking density such as eastern China, India, eastern and northern Europe, and eastern United States, where Y_{grazed} cannot fulfil the grass-biomass demand (Fig. 2a). Using the FAO-defined regions (see caption to Table 2), the largest fractions of managed grasslands are modelled in regions of high ruminant stocking density (Fig. S1) such as in eastern Europe with a mean fraction of $90 \pm 17\%$ (the mean is the average fraction of mown and grazed grasslands over all the grid cells in this region, and the standard deviation is taken from differences between grid cells), South Asia ($59 \pm 46\%$), and western Europe ($55 \pm 36\%$). The lowest managed grasslands fractions are modelled in the Russian Federation ($17 \pm 34\%$).

In some grid cells, the simulated grassland productivity is not sufficient to fulfil the grass-biomass use given by Herrero et al. (2013; Fig. 2d). Of the 2.4 billion tonnes of grass-biomass use (in dry matter for the reference year 2000) given by Herrero et al., 16 % cannot be fulfilled by the productivity simulated by ORCHIDEE-GM v3.1. This translates into a modelled grass-biomass production deficit of 0.38 billion tonnes (Table 2). Out of all regions, the largest modelled production deficit (f_{global} in Table 2) is found in South Asia (49 %). This South Asian deficit is predominantly in India (35 % of the modelled global total deficit) and Pakistan (10 % of the modelled global total deficit). Other regions with a biomass production deficit are the Near East and North Africa (18 %) and sub-Saharan Africa (13 %). Overall, 32 % of the global production deficit comes from regions with dry climate and low NPP (less than $50 \text{ g C m}^{-2} \text{ yr}^{-1}$), and 34 % of it comes from regions with low grassland cover (less than 10 % of total land cover). The causes of this grass-biomass production deficit diagnosed by ORCHIDEE-GM are discussed in Sect. 4.2.

Modelled herbage-use efficiency over managed grassland during the 2000s (grazed plus mown; Fig. 3) ranges between 2 and 20 % in most regions and generally follows the spatial pattern of grazing-ruminant density (Fig. S1). High herbage-use efficiency (over 20 %) is found in regions with significant mown grassland (f_{mown}) simulated due to the larger fraction of biomass removed over mown grassland than that over grazed grassland in the same grid cell (Fig. S3).

Figure 4 displays the NPP per unit area and the production ($\text{Prod} = \text{NPP} \times \text{grassland area}$) of each type of grassland for 10 FAO-defined regions and the globe. Even when grassland management is included, the production of unman-

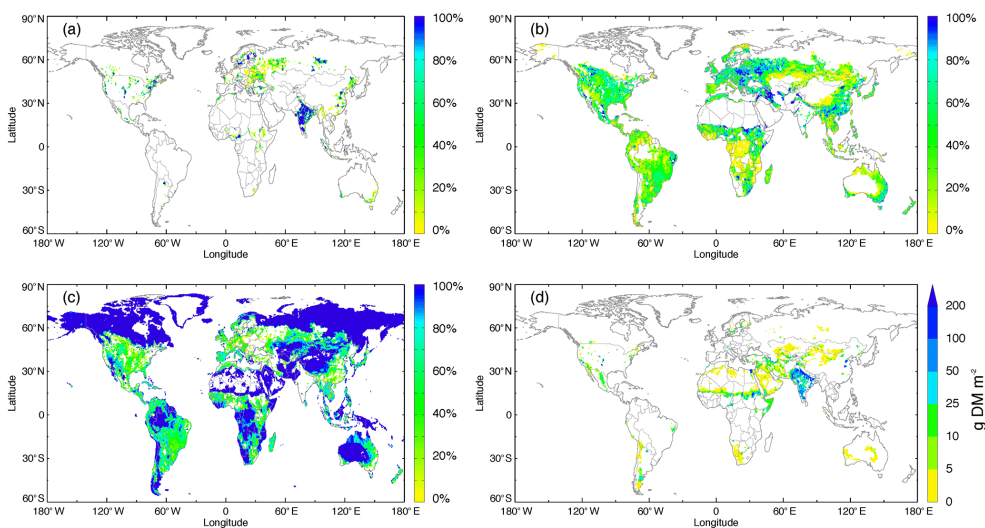


Figure 2. (a) Mown, (b) grazed, and (c) unmanaged fraction of global grassland, and (d) modelled grass-biomass production deficit of 2000. Modelled grass-biomass production deficit indicates the simulated grassland productivity in the grid cells is not sufficient to fulfil the grass-biomass use given by Herrero et al. (2013) and is expressed with units of g dry matter (DM) per m² of total land area in each grid cell.

Table 2. Grass-biomass production deficits in regions where simulated productivity by ORCHIDEE-GM v3.1 (i.e. Y_{mown} and Y_{grazed} ; see text) cannot fulfil the grass-biomass use given by Herrero et al. (2013) for 2000.

Regions ^a	Grass-biomass use (million tonne DM)	Production deficit (million tonne DM)	f_{deficit} (%) ^b	f_{global} (%) ^c
North America	228	19	8 %	5 %
Russian Federation	52	1	2 %	0.3 %
Western Europe	196	5	2 %	1 %
Eastern Europe	82	1	1 %	0.3 %
Near East and North Africa	175	67	39 %	18 %
East and Southeast Asia	275	25	9 %	7 %
Oceania	107	4	3 %	1 %
South Asia	390	188	48 %	49 %
Latin America and Caribbean	534	23	4 %	6 %
Sub-Saharan Africa	351	48	14 %	13 %
World total	2391	380	16 %	100 %

^a Regions are classified following the definition in the FAO Global Livestock Environmental Assessment Model (GLEAM; <http://www.fao.org/gleam/en/>).

^b f_{deficit} is the fraction of production deficit in the total grass-biomass use of the region for 2000.

^c f_{global} is the fraction of production deficit in the global total production deficit for 2000.

aged grassland ($\text{Prod}_{\text{unmanaged}}$) still comprises 63 % of the total production ($\text{Prod}_{\text{total}}$) in the 1990s. The production of grazed grasslands ($\text{Prod}_{\text{grazed}}$) accounts for 34 % of $\text{Prod}_{\text{total}}$, while the production of mown grasslands ($\text{Prod}_{\text{mown}}$) is only 3 %, given the small area under this management practice (Fig. 4). Mown grasslands only contribute to production in the regions where climate conditions and fertilizers maintain a high NPP, and Y_{grazed} is not enough to fulfil the animal requirement, which triggers the harvest practice in Eqs. (7–11).

Over unmanaged grassland (Fig. S2), ORCHIDEE-GM v3.1 simulated a total annual consumption by wild herbivores of 147–654 million tonnes DM of the 5778 million tonnes

DM in aboveground NPP (consumable NPP) over suitable grassland (Table S5), which comprises 3–11 % of the consumable NPP, similar to the range given by Warneck (1988). The fraction of consumption in consumable NPP varied from 1 % in the former USSR to 9 % in Scandinavia, indicating the different significance of wild herbivores on grassland.

3.2 Historical changes in the area and productivity of managed grassland

The global minimum area of managed grassland ($A_{\text{managed-gm}}$) is of $6.1 \times 10^6 \text{ km}^2$ in 1901 and increased to $12.3 \times 10^6 \text{ km}^2$ in 2000 (Table 3; Fig. 5) – an increase of

Table 3. Area, mean productivity, and herbage-use efficiency of managed grassland from this study, ruminant numbers, and pasture area from HYDE 3.1 dataset for 1901 and 2000 by regions and global total.

Regions ^a	Grassland area (1000 km ² ; 1901/2000)			Mean productivity (kg DM m ⁻² yr ⁻¹ ; 1900s/1990s ^b)		Herbage-use efficiency (Percent; 1900s/1990s)	N_{ruminant}^c (10 ⁶ LU; 1901/2000)	Pasture area from HYDE 3.1 ^d (1000 km ² ; 1901/2000)
	Total managed	Mown	Grazed	Y_{mown}	Y_{grazed}			
North America	989/1360	41/95	948/1265	0.26/0.38	0.09/0.13	6.2%/7.4%	42/87	1157/2482
Russian Federation	351/567	23/49	329/518	0.19/0.42	0.06/0.10	5.0%/5.8%	9/16	2995/904
Western Europe	514/555	54/44	460/522	0.51/0.85	0.22/0.31	10.0%/10.6%	49/76	793/595
Eastern Europe	339/366	71/93	268/274	0.26/0.54	0.11/0.21	7.1%/9.8%	12/17	655/248
Near East and North Africa	595/1334	17/130	578/1205	0.09/0.18	0.05/0.06	6.3%/6.2%	12/50	2607/5607
East and Southeast Asia	419/1271	6/77	412/1194	0.43/0.72	0.09/0.14	4.2%/5.8%	14/83	2998/5327
Oceania	499/828	52/60	447/769	0.18/0.33	0.07/0.11	7.2%/7.0%	11/33	979/4000
South Asia	614/830	123/202	491/628	0.32/0.58	0.10/0.12	10.4%/14.0%	35/109	651/962
Latin America and Caribbean	960/2640	11/33	949/2608	0.35/0.39	0.11/0.18	4.1%/5.2%	40/194	1341/5446
Sub-Saharan Africa	803/2561	8/109	795/2452	0.32/0.46	0.08/0.10	4.8%/5.5%	16/93	4486/6991
Global total	6083/12 313	404/891	5679/11 422	0.29/0.48	0.10/0.14	6.2%/6.6%	238/759	19 181/32 764

^a Regions are classified following the definition in the FAO Global Livestock Environmental Assessment Model (GLEAM; <http://www.fao.org/glead/en/>).

^b The potential harvested biomass from mown grassland (Y_{cut}) and the potential biomass consumption over grazed grassland (Y_{graze}) are 10-year averages for the period 1901–1910 (1900s) and 1991–2000 (1990s), representing the productivity at the beginning and at the end of the 20th century respectively.

^c Ruminant numbers (in units of livestock unit, LU) are calculated based on the total metabolisable energy (ME) requirement by all ruminant. The ME requirement by all ruminants is based on ruminant numbers from statistics (for 1961–2012; data derived from FAOSTAT, 2014) and literature estimates (for 1901–1960; data derived from Mitchell (1993, 1998a, b) and available in HYDE database at <http://thesites.pbl.nl/fridion/en/thesites/hyde/landusedata/livestock/index-2.html>), using the calculation method given in the Supplement Sect. S1 of Chang et al. (2015a).

^d See Klein Goldewijk et al. (2011) for details.

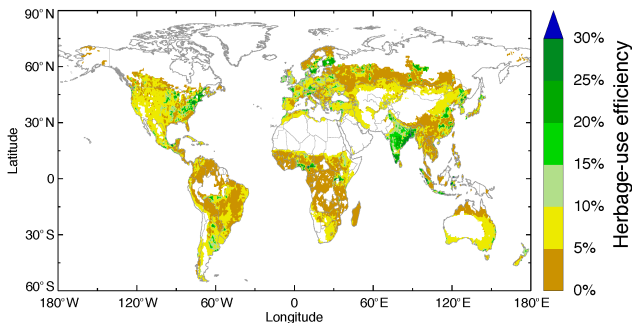


Figure 3. Average herbage-use efficiency over managed grassland (grazed plus mown) in 2000–2009 simulated by ORCHIDEE-GM v3.1. Herbage-use efficiency (Hodgson, 1979) is defined as the forage removed expressed as a proportion of herbage growth. In this study, the forage removed is modelled annual grass-biomass use including Y_{grazed} and Y_{mown} , and herbage growth is modelled annual grass GPP.

102 % during the 20th century. This expansion of managed grasslands is mainly explained by the increase in the area of grazed lands ($+5.7 \times 10^6 \text{ km}^2$), while mown grassland increased only marginally ($+0.5 \times 10^6 \text{ km}^2$). The largest extension of $A_{\text{managed-gm}}$ is found in sub-Saharan Africa ($+1.8 \times 10^6 \text{ km}^2$) and Latin America and the Caribbean ($+1.7 \times 10^6 \text{ km}^2$; Fig. 5). The regions with the largest relative expansion of managed grasslands (as a percentage of 1901 areas) are sub-Saharan Africa ($+219\%$), East and Southeast Asia ($+204\%$), and Latin America and the Caribbean ($+175\%$), and the regions where the number of domestic ruminants (N_{ruminant}) increased by nearly or over a factor of 3. Only small increases of $A_{\text{managed-gm}}$ were modelled in western Europe ($+41 \times 10^3 \text{ km}^2$; i.e. 8 %) and eastern Europe ($+27 \times 10^3 \text{ km}^2$; i.e. 8 %), despite an increase of N_{ruminant} by a factor of 1.5 in western Europe

($+27 \times 10^6 \text{ LU}$) and of 1.4 in eastern Europe ($+5 \times 10^6 \text{ LU}$). This means that livestock production intensified in those two regions, first by giving crop feedstock given to animals (Bouwman et al., 2005) and second through the optimization of forage harvesting and grazing to feed higher animal-stocking densities. Note that the animal density in eastern and western Europe peaked at $123 \times 10^6 \text{ LU}$ near 1990 and has declined by 29 % since then.

Besides the extension of managed grassland area, modelled herbage-use efficiency over managed grassland increased from 6.2 to 6.6 % during the 20th century, indicating the intensification of grassland management. Large increase in herbage-use efficiency is modelled in South Asia ($+3.6\%$) and eastern Europe ($+2.7\%$), while marginal decrease of herbage-use efficiency is found in the Near East and North Africa (-0.1%) and Oceania (-0.2% ; Table 3).

The global mean potential productivity of mown grassland (Y_{mown}) increased by 62 % from $0.29 \text{ kg DM m}^{-2} \text{ yr}^{-1}$ for 1900s to $0.48 \text{ kg DM m}^{-2} \text{ yr}^{-1}$ for the 1990s, while that of grazed grassland Y_{grazed} increased by 40 %, from $0.10 \text{ kg DM m}^{-2} \text{ yr}^{-1}$ for the 1900s to $0.14 \text{ kg DM m}^{-2} \text{ yr}^{-1}$ for the 1990s (Table 3). During the last century, Y_{mown} increased by more than 40 % in most regions except in Latin America and the Caribbean (14 %), while the increase of Y_{grazed} ranged from 25 % in sub-Saharan Africa and 80 % in eastern Europe (Table 3).

3.3 Evaluation of modelled productivity

Figure 6 shows the grassland productivity ($\text{NPP}_{\text{model}}$; Fig. 6a) and the NPP differences between $\text{NPP}_{\text{model}}$ and NPP from unmanaged grassland (Fig. 6b). The effect of including management does not produce a big difference in simulated NPP, which has similar patterns in most regions (Fig. 6b). Nevertheless, there are significant differences of NPP due to management in the central United States, Europe, northeast-

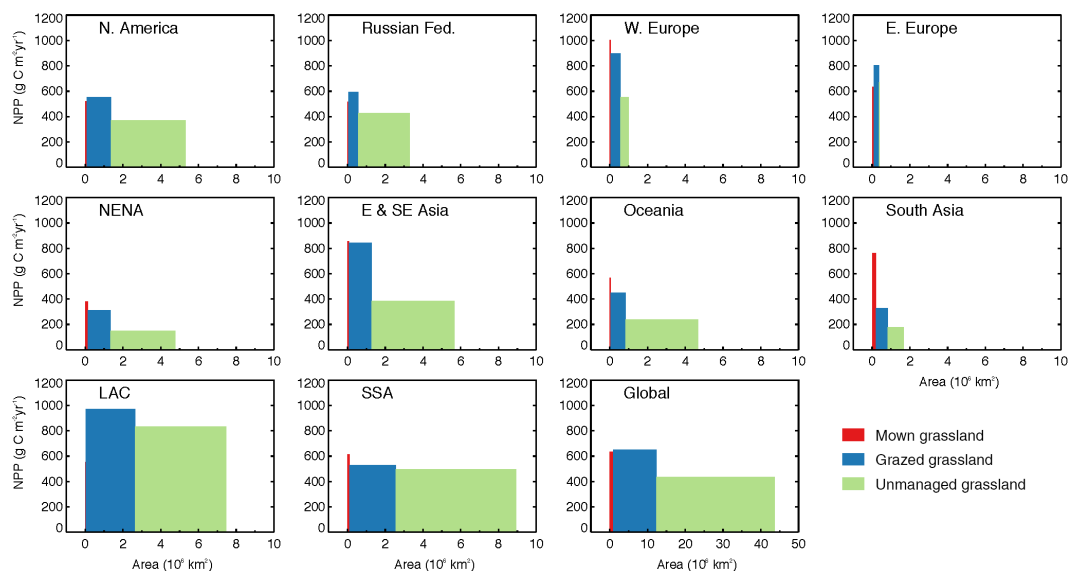


Figure 4. Productivities per unit area (height of each rectangle) and grassland areas (width of each rectangle) of the different types of grassland (mown, grazed, and unmanaged grassland) by FAO-defined regions and global total. Areas in the graph show the production of each grassland type (i.e. $Prod_{mown}$, $Prod_{grazed}$, and $Prod_{unmanaged}$; see Sect. 3.1 for detail). Productivities and grassland areas are averaged for 1991–2000. The FAO-defined regions (from top-left) are North America, Russian Federation, western Europe, eastern Europe, Near East and North Africa (NENA), East and Southeast Asia, Oceania, South Asia, Latin America and the Caribbean (LAC), and sub-Saharan Africa (SSA).

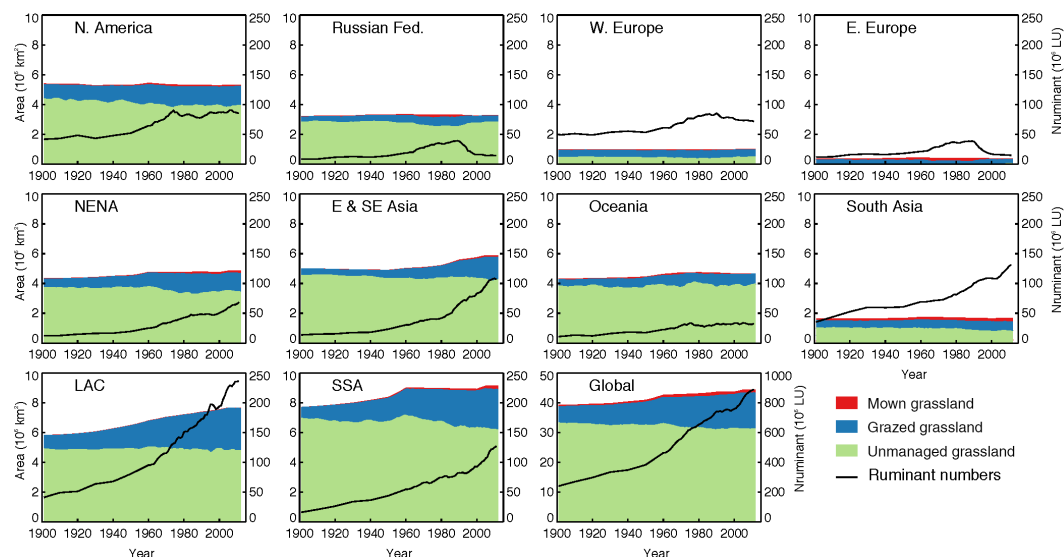


Figure 5. Historical changes in the area of managed/unmanaged grassland and in the ruminant numbers for 1901 and 2012 by region and global total. See caption to Table 2 for expansion of FAO-defined regions.

ern India, southern China, South Korea, Japan, and southern Brazil where N fertilizer additions (Tables S3 and S4) cause a higher productivity (Fig. 6b).

3.3.1 Evaluation of modelled NPP against observed NPP

Figure 7a shows the comparison between site-scale NPP observations (NPP_{obs}) and the model results at the corresponding grid cells (NPP_{model}). The NPP_{model} is positively correlated with NPP_{obs} across 129 sites but with the low cor-

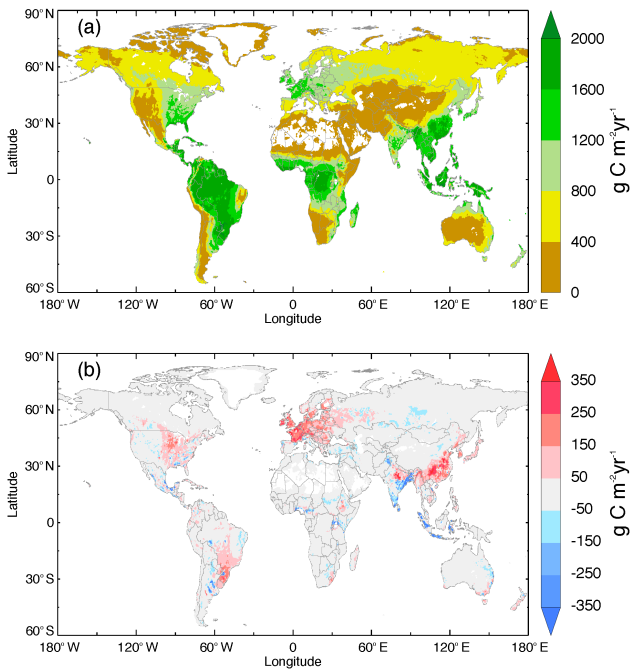


Figure 6. Modelled mean grassland NPP (NPP_{model}) for the period 1990–1999 (a), and the NPP differences (b) between NPP_{model} and NPP from unmanaged grassland only. NPP_{model} combines grassland productivity of all PFTs (Sect. 2.5), accounting for the variable fractions of grazed, mown, and unmanaged grassland in each grid cell calculated by Eqs. (4)–(11).

relation coefficient of $r = 0.35$ ($p < 0.01$) and the RMSE of $380 \text{ g C m}^{-2} \text{ yr}^{-1}$. Figure 7b presents box-and-whisker plot of the observed and modelled annual whole-plant NPP, aboveground NPP, and belowground NPP. The mean value and range of modelled whole-plant NPP are both higher than those of NPP_{obs} . The NPP overestimation by the model is mainly due to a too-high aboveground NPP, while belowground NPP is only little higher for its mean or even lower for its median than belowground NPP_{obs} .

3.3.2 Evaluation of modelled GPP against MODIS-GPP for annual mean and interannual variability

At global scale, MODIS-GPP gives a mean grassland GPP of $537 \text{ g C m}^{-2} \text{ yr}^{-1}$ and ORCHIDEE-GM v3.1 simulates a mean value of $796 \text{ g C m}^{-2} \text{ yr}^{-1}$, $\approx 50\%$ higher than MODIS-GPP. A higher modelled GPP (GPP_{model}) than MODIS is found for all latitude bands especially in boreal ($50\text{--}80^\circ \text{ N}$) and tropical regions ($20^\circ \text{ S--}20^\circ \text{ N}$; Fig. 8). The linear regression between gridded MODIS-GPP and GPP_{model} suggests a similar spatial pattern (slope = 1.05, and the correlation coefficient $r_{\text{spatial}} = 0.84$; Fig. S5).

The temporal correlation coefficient between the detrended time series of global GPP_{model} and MODIS-GPP was found to be high ($r_{1\text{AV-global}} = 0.88$, $p < 0.01$). Within the grid

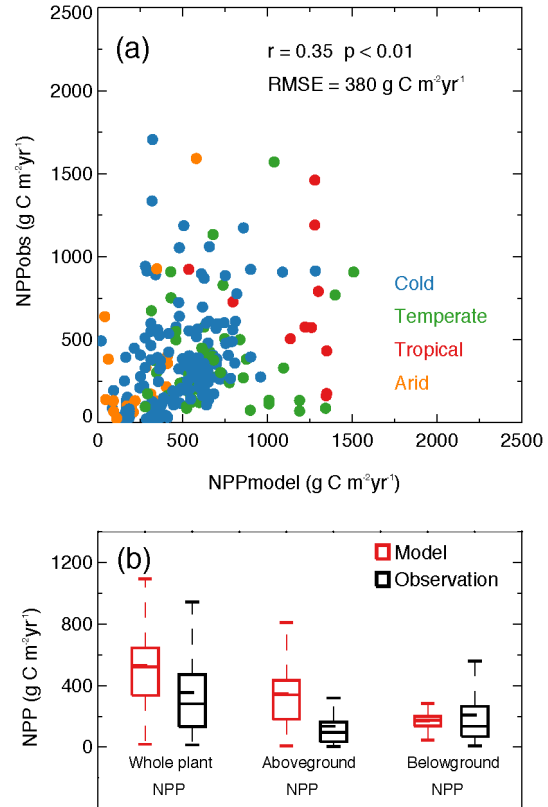


Figure 7. (a) Comparison between site observations of whole-plant NPP (NPP_{obs}) and modelled NPP (NPP_{model}); (b) box-and-whisker plot of the observed and modelled annual whole-plant NPP, aboveground NPP, and belowground NPP. In subplot (a), grassland sites in different Köppen climate zones are specified by different colours. The Köppen climate zones are classified based on Peel et al. (2007) using climate data from WorldClim (<http://www.worldclim.org/>). In subplot (b), the “whisker” indicates the cross-measurement (total 270 measurements) uncertainty.

cells covered by grass over more than 20% of total land in MOD12Q1, significant positive interannual correlations between GPP_{model} and MODIS-GPP were found for 39% of the grid cells (i.e. 40% of the grassland area), except in some tundra areas of Siberia and North America, grassland on the Qinghai–Tibet Plateau, and savannah in sub-Saharan Africa (Fig. 9).

3.3.3 Evaluation of modelled seasonal cycle of GPP against MODIS-GPP and GOME-2 SIF products

Figure 10 compares the normalized seasonal variation of GPP_{model} , MODIS-GPP, and SIF-GPP for five latitude bands and the globe. Similar mean seasonal variations of grassland productivity are found between modelled GPP, MODIS-GPP, and SIF (r_{seasonal} range from 0.55 to 0.89; Table 4). Compared to both MODIS-GPP and SIF data, ORCHIDEE-GM v3.1 captures the seasonal variation of productivity in bo-

Table 4. Mean \pm standard deviation of r_{seasonal} comparing the seasonal cycle of modelled GPP ($\text{GPP}_{\text{model}}$), MODIS-GPP, and SIF data for the five latitude bands and global scale. r_{seasonal} is expressed as mean \pm standard deviation of grid level correlation coefficient within each latitude band and global. To avoid the strong impact of other land-cover types (e.g. crop and forest) to the seasonal cycle, we only consider r_{seasonal} for grid cells with grassland covering more than 50% of total land in the MOD12Q1 dataset.

r_{seasonal}	Latitude bands					Global
	60–90° N	30–60° N	0–30° N	0–30° S	30–60° S	
$\text{GPP}_{\text{model}}$ vs. SIF data	0.84 ± 0.15	0.81 ± 0.19	0.66 ± 0.27	0.68 ± 0.28	0.55 ± 0.33	0.77 ± 0.23
$\text{GPP}_{\text{model}}$ vs. MODIS-GPP	0.89 ± 0.10	0.86 ± 0.16	0.71 ± 0.30	0.63 ± 0.44	0.63 ± 0.31	0.80 ± 0.27
MODIS-GPP vs. SIF data	0.90 ± 0.11	0.87 ± 0.16	0.80 ± 0.22	0.61 ± 0.37	0.61 ± 0.36	0.81 ± 0.25

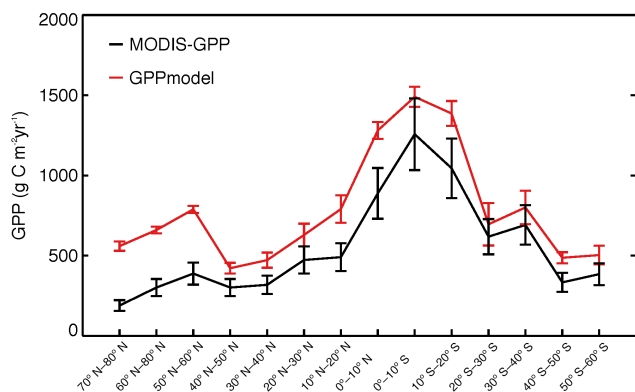


Figure 8. Comparison between mean MODIS-GPP and modelled GPP for the period 2000–2013 by latitude band. The uncertainty of MODIS-GPP comes from the reported relative error term driven by NASA’s Data Assimilation Office (DAO) reanalysis datasets (Zhao et al., 2006). The uncertainty of modelled GPP is the standard deviation of interannual variation of grassland GPP in each band for the period 2000–2013.

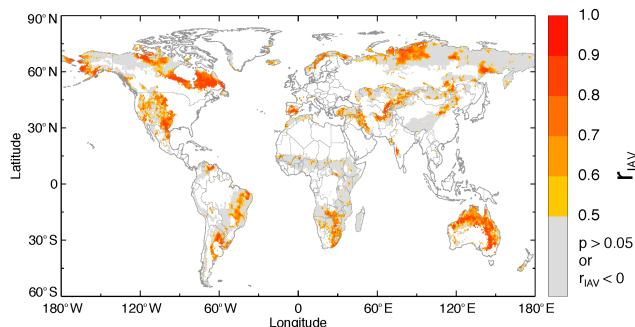


Figure 9. Spatial distribution of $r_{\text{I}\Delta\text{V}}$ between MODIS-GPP and $\text{GPP}_{\text{model}}$. $r_{\text{I}\Delta\text{V}}$ is the correlation coefficient between detrended time series of modelled and MODIS-GPP from 2000 to 2012. This figure only shows the $r_{\text{I}\Delta\text{V}}$ for grid cells with grassland covering more than 20% of total land in the MOD12Q1 dataset. Grey indicates insignificant or negative $r_{\text{I}\Delta\text{V}}$ ($p > 0.05$ or $r_{\text{I}\Delta\text{V}} < 0$); yellow-to-red indicates significant positive $r_{\text{I}\Delta\text{V}}$ with increasing value ($r_{\text{I}\Delta\text{V}} > 0$ and $p < 0.05$).

real and temperate regions of the Northern Hemisphere well ($r_{\text{seasonal}} > 0.8$; Table 4). In the band from 60° S to 30° N, relatively low average r_{seasonal} correlations are found both with MODIS-GPP and SIF (ranging from 0.55 to 0.71). However, note that the r_{seasonal} between the two remote sensing GPP related products is relatively low for grassland between 60° S and 30° N, particularly between 0 and 60° S (Table 4).

4 Discussion

4.1 Managed area of grassland and management intensity: comparison with previous estimates

The area of managed grasslands obtained in this study is lower than the pasture area of HYDE 3.1 ($A_{\text{pasture-hyde}}$, Klein Goldewijk et al., 2011; Table 3), except in eastern Europe for the year 2000. $A_{\text{pasture-hyde}}$ is 3.2 times larger than the minimum area of managed grasslands (mown plus grazed grasslands; hereafter referred to as $A_{\text{managed-gm}}$) in the year 1901 and 2.7 times larger in the year 2000. The difference comes from the method used for estimating managed areas between Klein Goldewijk et al. (2011) and this study. $A_{\text{pasture-hyde}}$ in Klein Goldewijk et al. (2011) was estimated simply from population density and the country-level-per-capita use of pasture derived from the FAO statistics (FAO-STAT, 2008). In this study, $A_{\text{managed-gm}}$ is constrained by grass-biomass-use data (i.e. requirement of biomass for animals) and the simulated grassland productivity (i.e. supply of biomass to animals). In fact, the actual (real-world) managed grassland area could be larger than $A_{\text{managed-gm}}$ in regions where grasslands are not strictly unmanaged, i.e. not fully occupied by $A_{\text{managed-gm}}$ in the management intensity maps (i.e. $f_{\text{unmanaged}} > 0$; Fig. 2c). In pastoral systems such as open rangeland and mountain areas, animals keep moving to search for the most digestible grass. Tracts of grasslands can be grazed for a short period, with only a small part of the annual grass productivity being digested (i.e. very low herbage-use efficiency). This type of grassland could be recognized as extensively grazed grassland, whereas it is considered as unmanaged in this study. For example, lower herbage-use efficiency than that simulated in this study (Fig. 3) could be expected in open rangeland of central Asia, the Rus-

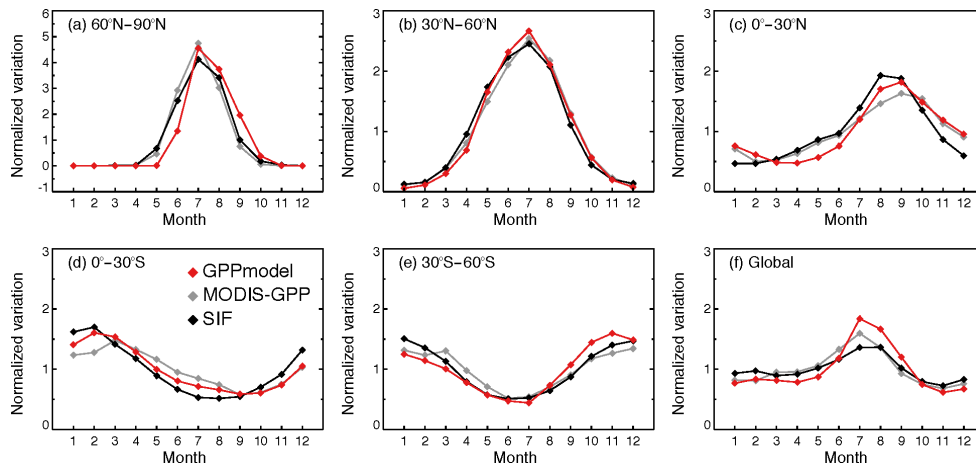


Figure 10. The normalized seasonal variation of modelled GPP (GPP_{model}), MODIS-GPP, and SIF for five latitude bands (a–e) and (f) global average.

sia federation, sub-Saharan Africa, Brazil, and Australia and in the mountains of southwestern China and the European Alps. Reclassifying these areas would result in a larger area of extensively managed grassland. Few studies reported the herbage-use efficiency of managed grassland. One exception is the network of European eddy-covariance flux sites. For these sites the average herbage-use efficiency (expressed as forage defoliated as a proportion of GPP) is $7.1\% \pm 6.1\%$ for grazed sites, and $13.3\% \pm 6.4\%$ for mown sites (J.-F. Soussana, personal communication, 2015); a similar range, between 2 and 20%, is simulated in this study (Fig. 3).

The time evolution of $A_{\text{managed-gm}}$ since 1901 in this study is arguably more realistic than HYDE because it considers changes in animal stocking density from statistics and the evolution in per-head use of pasture. $A_{\text{managed-gm}}$ takes into account (1) changes in grass-biomass requirement, considering both ruminant numbers and meat/milk productivity (Supplement Sect. S2; N_{ruminant} in Table 3); (2) changes in grassland productivity driven by climate change, rising CO_2 concentration, and changes in N fertilization (Y_{mown} and Y_{grazed} in Table 3); and (3) changes in management types (mown and grazed grassland areas in Table 3 and Fig. 5). For example in intensively managed grasslands, an increase in ruminant stocking density causes a shift from grazed to mown grassland (globally and regionally, except in western Europe; Table 3 and Fig. 5), because mown grassland provides more grass biomass than grazed grassland per unit of area (Fig. S3).

$A_{\text{pasture-hyde}}$ is consistent with country-specific pasture area censuses and thus may be suitable for reconstructing land cover, but it does not provide information about management intensity. $A_{\text{managed-gm}}$ and its split between mown, grazed, and unmanaged fractions provide specific global distributions of pasture management intensity and its historical changes. However, there are several limitations, which may

cause uncertainties in our maps of management intensity: (1) the grass fraction in ruminant diet has likely been changing during the last century while, due to a lack of information, we assumed that it was static in each region up to the year 2000; (2) technical developments (such as ruminant breeding) are not considered but may affect the feeding efficiency (meat/milk production per amount of feed) and thus feedback on the grass-biomass requirement; (3) the spatial distribution of ruminants was kept constant in our estimate, whereas it could have changed, depending on geographic changes in human population distribution; and (4) the results depend on the accuracy of NPP modelling in ORCHIDEE-GM. Despite these limitations, the maps of grassland management intensity provide new information for drawing up global estimates of management impact on biomass production and yields (Campioli et al., 2015) and for global vegetation models like ORCHIDEE-GM to enable simulations of carbon stocks and GHG budgets beyond simple tuning of grassland productivities (e.g. like in LPJmL; Bondeau et al., 2007) to account for management. These maps can also be tested in other vegetation models, or the same algorithm can be implemented in other models to give the management intensity consistent with simulated NPP.

4.2 Causes of regional grass-biomass production deficits

Grass-biomass production is constrained by the gridded biomass consumption for the year 2000 (Herrero et al., 2013). In some grid cells, the gridded biomass consumption by year 2000 cannot be fulfilled by the potential grass production simulated by ORCHIDEE-GM v3.1 (Fig. 2d). These modelled grass-biomass production deficits could be due to several reasons.

- Land-cover maps used as input to ORCHIDEE-GM v3.1 do not represent grasslands well in the mixed and landless systems and grasslands providing occasional feed to ruminant (e.g. roadside, forest understory grazing land, and small patches). This failing could cause the model to miss a significant part of grass productivity in this study. For example, the largest modelled grass-biomass production deficit is found in India because the simulated grassland productivity is far from agreeing with the grass-biomass-use data. In this country, occasional feed may constitute an important fraction of ruminant diet (30 or 50 % in mixed and landless or pastoral systems of South Asia from Bouwman et al., 2005), which is not represented by the land-cover maps used as input to ORCHIDEE-GM v3.1 and thus is not modelled.
- In arid regions such as Pakistan, Sudan, Iran, Egypt, and northwestern China, grass can grow in places where the water table is near to the surface and groundwater resources are available (e.g. oases, riparian zones, lakes). However, ORCHIDEE-GM v3.1 is driven by gridded climate data and does not taken into account local topography-dependent water resources such as rivers and lakes and thus is not being able to simulate local grass growing areas in arid regions.
- Grassland irrigation, though it is not as common as in cropland, is applied in arid regions such as Saudi Arabia but is not considered by ORCHIDEE-GM v3.1.
- In some semi-arid open rangeland, ruminants may walk long distances to acquire enough grass. For example, in semi-arid sub-Saharan Africa, Uzbekistan, and central Australia, animals usually keep moving in order to search for grass. This displacement of grazing animals from grass sources is not considered in the model.
- The grass fraction in ruminant diet is defined per region according to specific production systems. However, the grass fraction can differ within a region depending on local fodder crop production and grassland use. For example, the large numbers of ruminants in eastern China are mostly fed by grain and stovers (fibrous crop residues) instead of grass, because little grassland exists in that region.

4.3 Model performance: comparison of modelled and observed grassland productivity

In Sect. 3.3, the spatial patterns of NPP_{model} or GPP_{model} were compared with observations (NPP_{obs} or MODIS-GPP). ORCHIDEE-GM v3.1 captured well the spatial pattern of grassland productivity, with (i) high r_{spatial} between GPP_{model} and MODIS-GPP (Sect. 3.3.2) and (ii) NPP_{model} extracted from global simulation showing significant correlation with site-level NPP observation from 129 sites all over

the world (Sect. 3.3.1). However, GPP_{model} is higher than MODIS-GPP in all latitude bands (Fig. 8). It should be kept in mind that MODIS-GPP had a calculated 18 % uncertainty due to climate forcing (Zhao et al., 2006). Besides, a low bias of MODIS-GPP for grasslands has been reported in a tallgrass prairie in the United States (Turner et al., 2006) and in an alpine meadow on the Tibetan Plateau (Zhang et al., 2008) when compared to the GPP from flux-tower measurements. The underestimate of MODIS-GPP is mostly related to the low value of the maximum light-use efficiency parameters used in the MODIS-GPP algorithm (Turner et al., 2006; Zhang et al., 2008).

The relatively low r value between NPP_{model} and site-level NPP_{obs} ($r = 0.35$, $p < 0.01$; Sect. 3.3.1) could be related to the fact that local climate, soil properties, and topographic features are not considered in the model. For example, the r between the site-level climate and that from the CRU+NCEP climate forcing data ($0.5^\circ \times 0.5^\circ$ resolution) is 0.96 for annual mean temperature but only 0.86 for annual total precipitation and 0.86 for solar radiation. The relatively low correlation for annual total precipitation may cause inaccuracy in the model simulations of productivity, because water availability could be a major factor limiting grass growth (e.g. in temperate regions; Le Houerou et al., 1988; Silvertown et al., 1994; Briggs and Knapp 1995; Knapp et al., 2001; Nippert et al., 2006; Harpole et al., 2007). Further, a similar mean belowground NPP and an overestimation of mean aboveground NPP by ORCHIDEE-GM v3.1 is found in Sect. 3.3.1, which suggests that (1) the model tends to overestimate aboveground NPP possibly due to overestimation of GPP (compared to MODIS-GPP) and (2) the model tends to overestimate the ratio of aboveground and belowground biomass allocation ($R_{\text{above/below}}$) compared to observation. This overestimation could be the result of nitrogen limitation on the carbon allocation scheme for grassland. For example, a large nitrogen supply has been observed to increase $R_{\text{above/below}}$ (Aerts et al., 1991; Cotrufo and Gorissen, 1997), while nitrogen limitation might cause it to decrease. However, nitrogen limitation in grassland is not accounted for in ORCHIDEE-GM v3.1, which possibly leads to the model's overestimation of $R_{\text{above/below}}$. The model could be improved by incorporating the full nitrogen cycle.

For the seasonal cycle, we compared modelled GPP seasonality to both MODIS-GPP and GOME-2 SIF data. ORCHIDEE-GM v3.1 captures the seasonal variation of productivity in most regions where grassland is the dominant ecosystem (coverage $> 50\%$), as shown by the high r_{seasonal} between GPP_{model} and MODIS-GPP (Fig. S6a) or SIF data (Fig. S6b). However, the model does not capture the seasonal amplitude of grassland productivity in some arid/semi-arid regions (e.g. southwestern United States and central Australia; Fig. S6a and b). In arid/semi-arid regions, grass productivity is triggered by discrete precipitation events and depends on the timing and magnitude of these pulses (Sala et al., 1982; Schwinning and Sala, 2004; Huxman et al., 2004).

These precipitation pulses are infrequent, discrete, and not represented in a global climate re-analysis dataset such as CRU+NCEP used in our simulation. In particular, NCEP, like all climate models tends to produce “general circulation model drizzle” (Berg et al., 2010), i.e. too many frequent small rainfall events. This forcing uncertainty could be a major obstacle for our model to capture the seasonality of productivity in these regions. In dry grasslands, the dominant species could change during the season, but the resultant changes in SLA and $V_{c_{max}25}$ by different dominant species cannot be reflected in ORCHIDEE-GM v3.1. This within-season variability could be another reason for the model–data discrepancy in arid/semi-arid grassland seasonality. For the savanna of sub-Saharan Africa, eastern Africa, and South America (Fig. S6), the relatively low $r_{seasonal}$ could be a result of the fact that the frequent fires are not simulated in the current version of the model used here.

ORCHIDEE-GM v3.1 captures the IAV of grassland GPP at global scale and in many regions of the world (40 % of global grassland area) compared to the MODIS-GPP. One exception where IAV is not in phase with MODIS-GPP is sub-Saharan Africa (Fig. 9). Possible causes of this discrepancy are (1) the frequent fires which affect the IAV of GPP, which are not simulated in this study; (2) model biases in the IAV of soil moisture, which could affect the model performances for the productivity of semi-arid Africa, given its two-layer bucket hydrology; (3) the problems with MODIS-GPP dry areas, which may degrade the model–data agreement. The cold Qinghai–Tibet plateau and boreal tundra are the other regions where the model does not capture the GPP IAV (Fig. 9). The low model–data agreement in IAV could be due to shortcomings in (1) the specific characteristics, functioning traits, and nutrient availability of the tundra/alpine-grassland ecosystem that are not well parameterized or accounted for in our model (e.g. Tan et al., 2010, for Qinghai–Tibet plateau) and (2) the snow scheme. The timing of snowmelt will impact the grass phenology, while early spring soil moisture impacted by snow water storage may affect the grassland productivity. The single-bucket snowpack scheme (Chalita and Le Treut, 1994) in the current version of ORCHIDEE-GM may not represent the snow processes sufficiently accurately. The mechanistic intermediate-complexity snow scheme (ISBA-ES; Boone and Etchevers, 2001) implemented into ORCHIDEE-ES (Wang et al., 2013) may improve the model performance in simulating grassland productivity.

5 Concluding remarks

In this study, we have derived the global gridded maps of grassland management intensity, including the minimum area of managed grassland with fraction of mown/grazed part, the grazing-ruminant stocking density, and the density of the wild animal population at a resolution of 0.5°

by 0.5° . The management intensity maps are built based on the assumption that grass-biomass production from managed grassland (simulated by ORCHIDEE-GM v3.1) in each grid cell is just enough to satisfy the grass-biomass requirement by ruminants in the same grid (data derived from Herrero et al., 2013). Furthermore, the maps are extended to cover the period 1901–2012, taking into account both the changes in grass-biomass requirement and supply. The evolution in grass-biomass requirement is determined by the ME-based ruminant numbers calculated in this study, while the changes in grass-biomass supply are simulated by ORCHIDEE-GM v3.1, considering variable drivers such as climate, CO_2 concentration, and N fertilization. Despite the multiple sources of uncertainty, these maps, to our knowledge for the first time, provide global, time-dependent information on grassland management intensity. Global vegetation models such as ORCHIDEE-GM, containing an explicit representation of grassland management, are now able to use these maps to make a more accurate estimate of global carbon and GHG budgets.

The gridded grassland management intensity maps are model dependent because they depend on NPP. Thus in this study we also give a specific attention to the evaluation of modelled productivity against both a new set of site-level NPP measurements and global satellite-based products (MODIS-GPP and GOME2-SIF). Generally, ORCHIDEE-GM v3.1 captures the spatial pattern, seasonal cycle, and IAV of grassland productivity at global scale, except in regions with either arid or cold climates (tundra) and high-altitude mountains/plateaus. Because the major purpose of a global vegetation model like ORCHIDEE-GM is to simulate carbon, water, and energy fluxes at a large scale, it uses a limited number of plant functional types and generic equations. The model is not expected to accurately capture productivity variations everywhere. Thus we conclude that its current version, ORCHIDEE-GM v3.1, is suitable to simulate global grassland productivity.

6 Data availability

The ORCHIDEE model used as a starting point in this study is ORCHIDEE rev2425. The source code can be obtained at <http://forge.ipsl.jussieu.fr/orchidee/browser/trunk#ORCHIDEE>. A detailed documentation and the forcing data needed to drive ORCHIDEE can be found at <http://forge.ipsl.jussieu.fr/orchidee/wiki/Documentation> and <http://forge.ipsl.jussieu.fr/orchidee/wiki/Forcings>. ORCHIDEE-GM v3.1 is derived from rev2425 with the modifications presented in Sect. 2.1 and the previous studies (Chang et al., 2013, 2015a, b), the source code of which can be obtained upon request (<http://labex.ipsl.fr/orchidee/index.php/contact>).

CRU-NCEPv4 climate forcing is available at <http://dods.extra.cea.fr/data/p529viov/cruncep/readme.htm>. The EC-JRC-MARS database (European Commission – Joint

Research Center – Monitoring Agricultural ResourceS) can be accessed at <https://ec.europa.eu/jrc/en/mars>. The data on ruminant numbers come from several sources: for the period 1961–2012, data were derived from FAO-STAT (2014) (<http://faostat3.fao.org/>); for the period 1901–1960, data were available from the HYDE database at <http://themasites.pbl.nl/tridion/en/themasites/hyde/landusedata/livestock/index-2.html> and derived from literature estimates by Mitchell (1993, 1998a, b). The Köppen climate zones are classified based on Peel et al. (2007) using climate data from WorldClim (Hijmans et al., 2005; available at <http://www.worldclim.org/>).

The Supplement related to this article is available online at doi:10.5194/bg-13-3757-2016-supplement.

Acknowledgements. We thank the editor and the two anonymous referees for their valuable review comments, which helped to greatly improve the paper. We gratefully acknowledge funding from the European Union Seventh Framework Programme FP7/2007–2013 under grant no. 603864 (HELIX). Philippe Ciais and Shushi Peng acknowledge support from the ERC Synergy grant ERC-2013-SyG-610028 IMBALANCE-P. Matteo Campioli is a postdoctoral fellow at the Research Foundation – Flanders (FWO). Chao Yue is supported by the European Commission-funded project LUC4C (grant no. 603542). Tao Wang is funded by European Union FP7-ENV project PAGE21 (grant no. 282700). We thank those who developed the EC-JRC-MARS dataset (©European Union, 2011–2014) created by MeteoConsult based on ECWMF (European Centre for Medium Range Weather Forecasts) model outputs and a reanalysis of ERA-Interim. We greatly thank John Gash for his effort on English language editing.

Edited by: A. Ito

References

- Aerts, R., Boot, R. G. A., and Van der Aart, P. J. M.: The relation between above- and belowground biomass allocation patterns and competitive ability, *Oecologia*, 87, 551–559, 1991.
- Bartholomé, E. and Belward, A.: GLC2000: a new approach to global land cover mapping from Earth observation data, *Int. J. Remote Sens.*, 26, 1959–1977, 2005.
- Berg, A., Sultan, B., and de Noblet-Ducoudré, N.: What are the dominant features of rainfall leading to realistic large-scale crop yield simulations in West Africa?, *Geophys. Res. Lett.*, 37, L05405, doi:10.1029/2009GL041923, 2010.
- Bondeau, A., Smith, P. C., Zaehle, S., Schaphoff, S., Lucht, W., Cramer, W., Gerten, D., Lotze-Campen, H., Mueller, C., Reichstein, M., and Smith, B.: Modelling the role of agriculture for the 20th century global terrestrial carbon balance, *Global Change. Biol.*, 13, 679–706, doi:10.1111/j.1365-2486.2006.01305.x, 2007.
- Boone, A. and Etchevers, P.: An intercomparison of three snow schemes of varying complexity coupled to the same land surface model: Local-scale evaluation at an Alpine site, *J. Hydrometeorol.*, 2, 374–394, 2001.
- Bouwman, A., Lee, D., Asman, W., Dentener, F., Van Der Hoek, K., and Olivier, J.: A global high-resolution emission inventory for ammonia, *Global Biogeochem. Cy.*, 11, 561–587, 1997.
- Bouwman, A., Boumans, L., and Batjes, N.: Estimation of global NH₃ volatilization loss from synthetic fertilizers and animal manure applied to arable lands and grasslands, *Global Biogeochem. Cy.*, 16, 8-1–8-14, 2002a.
- Bouwman, A., Boumans, L., and Batjes, N.: Modeling global annual N₂O and NO emissions from fertilized fields, *Global Biogeochem. Cy.*, 16, 28-21–28-29, 2002b.
- Bouwman, A. F., Van der Hoek, K. W., Eickhout, B., and Soenari, I.: Exploring changes in world ruminant production systems, *Agr. Syst.*, 84, 121–153, doi:10.1016/j.agry.2004.05.006, 2005.
- Briggs, J. M. and Knapp, A. K.: Interannual variability in primary production in tallgrass prairie – climate, soil-moisture, topographic position fire as determinants of aboveground biomass, *Am. J. Bot.*, 82, 1024–1030, doi:10.2307/2446232, 1995.
- Campioli M., Vicca S., Luysaert S., Bilcke, J., Ceschia, E., Chapin III, F. S., Ciais, P., Fernandez-Martinez, M., Malhi, Y., Obersteiner, M., Olefeldt, D., Papale, D., Piao, S. L., Peñuelas, J., Sullivan, P. F., Wang, X., Zenone, T., and Janssens, I. A.: Biomass production efficiency controlled by management in temperate and boreal ecosystems, *Nat. Geosci.*, 8, 843–846, doi:10.1038/NNGEO2553, 2015.
- Chalita, S. and Le Treut, H.: The albedo of temperate and boreal forest and the Northern Hemisphere climate: a sensitivity experiment using the LMD GCM, *Clim. Dynam.*, 10, 231–240, 1994.
- Chang, J., Ciais, P., Viovy, N., Vuichard, N., Sultan, B., and Soussana, J. F.: The greenhouse gas balance of European grasslands, *Global Change. Biol.*, 21, 3748–3761, 2015a.
- Chang, J., Viovy, N., Vuichard, N., Ciais, P., Campioli, M., Klumpp, K., Martin, R., Leip, A., and Soussana, J.-F.: Modeled Changes in Potential Grassland Productivity and in Grass-Fed Ruminant Livestock Density in Europe over 1961–2010, *PLoS ONE*, 10, e0127554, doi:10.1371/journal.pone.0127554, 2015b.
- Chang, J., Ciais, P., Viovy, N., Vuichard, N., Herrero, M., Havlík, P., Wang, X., Sultan, B., and Soussana, J. F.: Effect of climate change, CO₂ trends, nitrogen addition, and land-cover and management intensity changes on the carbon balance of European grasslands, *Global Change. Biol.*, 22, 338–350, doi:10.1111/gcb.13050, 2016.
- Chang, J. F., Viovy, N., Vuichard, N., Ciais, P., Wang, T., Cozic, A., Lardy, R., Graux, A.-I., Klumpp, K., Martin, R., and Soussana, J.-F.: Incorporating grassland management in ORCHIDEE: model description and evaluation at 11 eddy-covariance sites in Europe, *Geosci. Model Dev.*, 6, 2165–2181, doi:10.5194/gmd-6-2165-2013, 2013.
- Ciais, P., Reichstein, M., Viovy, N., Granier, A., Ogee, J., Allard, V., Aubinet, M., Buchmann, N., Bernhofer, C., Carrara, A., Chevalier, F., De Noblet-Ducoudré, N., Friend, A. D., Friedlingstein, P., Grunwald, T., Heinesch, B., Kerönen, P., Knohl, A., Krinner, G., Loustau, D., Manca, G., Matteucci, G., Miglietta, F., Ourcival, J. M., Papale, D., Pilegaard, K., Rambal, S., Seufert, G., Soussana, J. F., Sanz, M. J., Schulze, E. D., Vesala, T.,

- and Valentini, R.: Europe-wide reduction in primary productivity caused by the heat and drought in 2003, *Nature*, 437, 529–533, doi:10.1038/nature03972, 2005.
- Collatz, G. J., Ribas-Carbo, M., and Berry, J. A.: Coupled photosynthesis-stomatal conductance model for leaves of C4 plants, *Funct. Plant Biol.*, 19, 519–538, 1992.
- Cotrufo, M. F. and Gorissen, A.: Elevated CO₂ enhances below-ground C allocation in three perennial grass species at different levels of N availability, *New Phytol.*, 137, 421–431, 1997.
- European Commission – Joint Research Center: Monitoring Agricultural Resources: <https://ec.europa.eu/jrc/en/mars>, last access: December 2013.
- Eva, H. D., Belward, A. S., De Miranda, E. E., Di Bella, C. M., Gond, V., Huber, O., Jones, S., Sgrenzaroli, M., and Fritz, S.: A land cover map of South America, *Glob. Change. Biol.*, 10, 731–744, 2004.
- FAO: FAO Production Yearbook, Vol. 56, Rome, 2003.
- FAO: World agriculture: towards 2030/2050. Interim report, Global Perspective Studies Unit, Food and Agriculture Organization of the United Nations, Rome, Italy, 2006.
- FAO/IFA: Global estimates of gaseous emissions of NH₃, NO and N₂O from agricultural land, report, 106 pp., U.N./Int. Fertil. Ind. Assn., Rome, 2001.
- FAO/IFA/IFDC: Fertilizer use by crop, Fourth Edition, Rome, 1999.
- FAO/IFA/IFDC/IPI/PPI: Fertilizer use by crop, Fifth Edition, Rome, 64 pp., 2002.
- FAO: Food and Agriculture Organization of the United Nations (FAO), Rome, Italy, available at: <http://www.fao.org> (last access: October 2008), 2008.
- FAOstat: <http://faostat3.fao.org/> (last access: November 2014), 2014.
- Farquhar, G. D., von Caemmerer, S. V., and Berry, J. A.: A biochemical model of photosynthetic CO₂ assimilation in leaves of C3 species, *Planta*, 149, 78–90, 1980.
- Feng, X. and Dietze, M.: Scale dependence in the effects of leaf ecophysiological traits on photosynthesis: Bayesian parameterization of photosynthesis models, *New Phytol.*, 200, 1132–1144, 2013.
- Graux, A. I., Gaurut, M., Agabriel, J., Baumont, R., Delagarde, R., Delaby, L., and Soussana, J. F.: Development of the Pasture Simulation Model for assessing livestock production under climate change, *Agric. Ecosyst. Environ.*, 144, 69–91, doi:10.1016/j.agee.2011.07.001, 2011.
- Guanter, L., Zhang, Y., Jung, M., Joiner, J., Voigt, M., Berry, J. A., Frankenberg, C., Huete, A. R., Zarco-Tejada, P., Lee, J., Moran, M. S., Ponce-Campos, G., Beer, C., Camps-Valls, G., Buchmann, N., Gianelle, D., Klumpp, K., Cescatti, A., Baker, J. M., and Griffiths, T. J.: Global and time-resolved monitoring of crop photosynthesis with chlorophyll fluorescence, *P. Natl. Acad. Sci. USA*, 111, E1327–E1333, doi:10.1073/pnas.1320008111, 2014.
- Harpole, W. S., Potts, D. L., and Suding, K. N.: Ecosystem responses to water and nitrogen amendment in a California grassland, *Glob. Change. Biol.*, 13, 2341–2348, doi:10.1111/j.1365-2486.2007.01447.x, 2007.
- Hauglustaine, D. A., Balkanski, Y., and Schulz, M.: A global model simulation of present and future nitrate aerosols and their direct radiative forcing of climate, *Atmos. Chem. Phys.*, 14, 11031–11063, doi:10.5194/acp-14-11031-2014, 2014.
- Herrero, M., Havlik, P., Valin, H., Notenbaert, A., Rufino, M. C., Thornton, P. K., Blummel, M., Weiss, F., Grace, D., and Obersteiner, M.: Biomass use, production, feed efficiencies, and greenhouse gas emissions from global livestock systems, *P. Natl. Acad. Sci. USA*, 110, 20888–20893, doi:10.1073/pnas.1308149110, 2013.
- Hijmans, R. J., Cameron, S. E., Parra, J. L., Jones, P. G., and Jarvis, A.: Very high resolution interpolated climate surfaces for global land areas, *Int. J. Climatol.*, 25, 1965–1978, 2005.
- Hodgson, J.: Nomenclature and definitions in grazing studies, *Grass Forage Sci.*, 34, 11–17, 1979.
- Hurt, G., Chini, L. P., Frolking, S., Betts, R., Feddema, J., Fischer, G., Fisk, J., Hibbard, K., Houghton, R., and Janetos, A.: Harmonization of land-use scenarios for the period 1500–2100: 600 years of global gridded annual land-use transitions, wood harvest, and resulting secondary lands, *Clim. Change*, 109, 117–161, 2011.
- Huxman, T. E., Snyder, K. A., Tissue, D., Leffler, A. J., Ogle, K., Pockman, W. T., Sandquist, D. R., Potts, D. L., and Schwinning, S.: Precipitation pulses and carbon fluxes in semiarid and arid ecosystems, *Oecologia*, 141, 254–268, 2004.
- IFA (International Fertilizer Industry Association), Nitrogen-Phosphate-Potash, IFADATA statistics from 1973/74–1973 to 1997/98–1997 including separately world fertilizer consumption statistics, Paris, 1999.
- IPSL: ORCHIDEE, available at: <http://forge.ipsl.jussieu.fr/orchidee/browser/trunk#ORCHIDEE> (last access: January 2015), 2015.
- IPCC (Intergovernmental Panel on Climate Change): Climate change 2013: The Physical Scientific Basis (Contribution of Working Group I to the Fifth Assessment Report of the Intergovernmental Panel on Climate Change, 2013), Cambridge University Press, Cambridge, United Kingdom and New York, NY, USA, 2013.
- Joiner, J., Yoshida, Y., Vasilkov, A., Schaefer, K., Jung, M., Guanter, L., Zhang, Y., Garrity, S., Middleton, E., and Huemmrich, K.: The seasonal cycle of satellite chlorophyll fluorescence observations and its relationship to vegetation phenology and ecosystem atmosphere carbon exchange, *Remote Sens. Environ.*, 152, 375–391, 2014.
- Jung, M., Reichstein, M., Margolis, H. A., Cescatti, A., Richardson, A. D., Arain, M. A., Arneth, A., Bernhofer, C., Bonal, D., and Chen, J.: Global patterns of land-atmosphere fluxes of carbon dioxide, latent heat, and sensible heat derived from eddy covariance, satellite, and meteorological observations, *J. Geophys. Res.-Biogeosci.*, 116, G00J07, doi:10.1029/2010JG001566, 2011.
- Kattge, J., Díaz, S., Lavorel, S., et al.: TRY – a global database of plant traits, *Glob. Change Biol.*, 17, 2905–2935, doi:10.1111/j.1365-2486.2011.02451.x, 2011.
- Klein Goldewijk, K., Beusen, A., Van Drecht, G., and De Vos, M.: The HYDE 3.1 spatially explicit database of human-induced global land-use change over the past 12,000 years, *Global Ecol. Biogeogr.*, 20, 73–86, 2011.
- Knapp, A. K., Briggs, J. M., and Koelliker, J. K.: Frequency and extent of water limitation to primary production in a mesic temperate grassland, *Ecosystems*, 4, 19–28, doi:10.1007/s100210000057, 2001.

- Krinner, G., Viovy, N., de Noblet-Ducoudre, N., Ogee, J., Polcher, J., Friedlingstein, P., Ciais, P., Sitch, S., and Prentice, I. C.: A dynamic global vegetation model for studies of the coupled atmosphere-biosphere system, *Global Biogeochem. Cy.*, 19, GB1015, doi:10.1029/2003GB002199, 2005.
- Lamarque, J.-F., Bond, T. C., Eyring, V., Granier, C., Heil, A., Klimont, Z., Lee, D., Liousse, C., Mieville, A., Owen, B., Schultz, M. G., Shindell, D., Smith, S. J., Stehfest, E., Van Aardenne, J., Cooper, O. R., Kainuma, M., Mahowald, N., McConnell, J. R., Naik, V., Riahi, K., and van Vuuren, D. P.: Historical (1850–2000) gridded anthropogenic and biomass burning emissions of reactive gases and aerosols: methodology and application, *Atmos. Chem. Phys.*, 10, 7017–7039, doi:10.5194/acp-10-7017-2010, 2010.
- Le Houerou, H. N., Bingham, R. L., and Skerbek, W.: Relationship between the variability of primary production and the variability of annual precipitation in world arid lands, *J. Arid. Environ.*, 15, 1–18, 1988.
- Leip, A., Marchi, G., Koeble, R., Kempen, M., Britz, W., and Li, C.: Linking an economic model for European agriculture with a mechanistic model to estimate nitrogen and carbon losses from arable soils in Europe, *Biogeosciences*, 5, 73–94, doi:10.5194/bg-5-73-2008, 2008.
- Leip, A., Britz, W., Weiss, F., and de Vries, W.: Farm, land, and soil nitrogen budgets for agriculture in Europe calculated with CAPRI, *Environ. Pollut.*, 159, 3243–3253, doi:10.1016/j.envpol.2011.01.040, 2011.
- Leip, A., Weiss, F., Lesschen, J. P., and Westhoek, H.: The nitrogen footprint of food products in the European Union, *J. Agric. Sci.*, 152, S20–S33, doi:10.1017/s0021859613000786, 2014.
- Luyssaert, S., Inglisma, I., Jung, M., Richardson, A., Reichstein, M., Papale, D., Piao, S., Schulze, E. D., Wingate, L., and Matteucci, G.: CO₂ balance of boreal, temperate, and tropical forests derived from a global database, *Global Change. Biol.*, 13, 2509–2537, 2007.
- Martin, C., Morgavi, D. P., and Doreau, M.: Methane mitigation in ruminants: from microbe to the farm scale, *Animal*, 4, 351–365, doi:10.1017/s1751731109990620, 2010.
- Mitchell, B. R.: *International Historical Statistics, The Americas: 1750–1988*, New York, Stockton Press, London, MacMillan Publishers Ltd., 817 pp., 1993.
- Mitchell, B. R.: *International historical statistics Europe: 1750–1993*, Fourth Edition, New York, Stockton Press, London, MacMillan Reference Ltd., 959 pp., 1998a.
- Mitchell, B. R.: *International Historical Statistics, Africa, Asia and Oceania: 1750–1993*, Third Edition, New York, Stockton Press, London, MacMillan Reference Ltd., 1113 pp., 1998b.
- Mitchell, T. D. and Jones, P. D.: An improved method of constructing a database of monthly climate observations and associated high-resolution grids, *Int. J. Climatol.*, 25, 693–712, 2005.
- Nippert, J. B., Knapp, A. K., and Briggs, J. M.: Intra-annual rainfall variability and grassland productivity: can the past predict the future?, *Plant Ecol.*, 184, 65–74, 2006.
- PBL Netherlands Environmental Assessment Agency: HYDE database, available at: <http://themasites.pbl.nl/tridion/en/themasites/hyde/landusedata/livestock/index-2.html>, last access: December 2014.
- Peel, M. C., Finlayson, B. L., and McMahon, T. A.: Updated world map of the Köppen-Geiger climate classification, *Hydro. Earth Syst. Sci.*, 11, 1633–1644, doi:10.5194/hess-11-1633-2007, 2007.
- Peregon, A., Maksyutov, S., Kosykh, N. P., and Mironycheva-Tokareva, N. P.: Map-based inventory of wetland biomass and net primary production in western Siberia, *J. Geophys. Res.*, 113, G01007, doi:10.1029/2007JG000441, 2008.
- Piao, S., Friedlingstein, P., Ciais, P., de Noblet-Ducoudré, N., Labat, D., and Zaehle, S.: Changes in climate and land use have a larger direct impact than rising CO₂ on global river runoff trends, *P. Natl. Acad. Sci. USA*, 104, 15242–15247, doi:10.1073/pnas.0707213104, 2007.
- Poulter, B., Ciais, P., Hodson, E., Lischke, H., Maignan, F., Plummer, S., and Zimmermann, N. E.: Plant functional type mapping for earth system models, *Geosci. Model Dev.*, 4, 993–1010, doi:10.5194/gmd-4-993-2011, 2011.
- Riedo, M., Grub, A., Rosset, M., and Fuhrer, J.: A pasture simulation model for dry matter production, and fluxes of carbon, nitrogen, water and energy, *Ecol. Modell.*, 105, 141–183, doi:10.1016/s0304-3800(97)00110-5, 1998.
- Robinson, T. P., Wint, G. W., Conchedda, G., Van Boeckel, T. P., Ercoli, V., Palamara, E., Cinardi, G., D’Aielli, L., Hay, S. I., and Gilbert, M.: Mapping the global distribution of livestock, *PLoS ONE*, 9, e96084, doi:10.1371/journal.pone.0096084, 2014.
- Sala, O. and Lauenroth, W.: Small rainfall events: an ecological role in semiarid regions, *Oecologia*, 53, 301–304, 1982.
- Schwinning, S. and Sala, O. E.: Hierarchy of responses to resource pulses in arid and semi-arid ecosystems, *Oecologia*, 141, 211–220, 2004.
- Scurlock, J. M. O., Cramer, W., Olson, R., Parton, W., and Prince, S.: Terrestrial NPP: toward a consistent data set for global model evaluation, *Ecol. Appl.*, 9, 913–919, 1999.
- Scurlock, J. M. O., Johnson, K., and Olson, R. J.: Estimating net primary productivity from grassland biomass dynamics measurements, *Glob. Change Biol.*, 8, 736–753, doi:10.1046/j.1365-2486.2002.00512.x, 2002.
- Silvertown, J., Dodd, M. E., McConway, K., Potts, J., and Crawley, M.: Rainfall, biomass variation, and community composition in the park grass experiment, *Ecology*, 75, 2430–2437, doi:10.2307/1940896, 1994.
- Soussana, J. F., Allard, V., Pilegaard, K., Ambus, P., Amman, C., Campbell, C., Ceschia, E., Clifton-Brown, J., Czobel, S., Domingues, R., Flechard, C., Fuhrer, J., Hensen, A., Horvath, L., Jones, M., Kasper, G., Martin, C., Nagy, Z., Neftel, A., Raschi, A., Baronti, S., Rees, R. M., Skiba, U., Stefani, P., Manca, G., Sutton, M., Tubaf, Z., and Valentini, R.: Full accounting of the greenhouse gas (CO₂, N₂O, CH₄) budget of nine European grassland sites, *Agric. Ecosyst. Environ.*, 121, 121–134, doi:10.1016/j.agee.2006.12.022, 2007.
- Tan, K., Ciais, P., Piao, S., Wu, X., Tang, Y., Vuichard, N., Liang, S., and Fang, J.: Application of the ORCHIDEE global vegetation model to evaluate biomass and soil carbon stocks of Qinghai-Tibetan grasslands, *Global Biogeochem. Cy.*, 24, GB1013, doi:10.1029/2009GB003530, 2010.
- Turner, D. P., Ritts, W. D., Cohen, W. B., Gower, S. T., Running, S. W., Zhao, M., Costa, M. H., Kirschbaum, A. A., Ham, J. M., and Saleska, S. R.: Evaluation of MODIS NPP and GPP products across multiple biomes, *Remote Sens. Environ.*, 102, 282–292, 2006.

- Verheijen, L. M., Brovkin, V., Aerts, R., Bönisch, G., Cornelissen, J. H. C., Kattge, J., Reich, P. B., Wright, I. J., and van Bodegom, P. M.: Impacts of trait variation through observed trait-climate relationships on performance of an Earth system model: a conceptual analysis, *Biogeosciences*, 10, 5497–5515, doi:10.5194/bg-10-5497-2013, 2013.
- Viovy, N.: CRU-NCEPv4, CRUNCEP dataset, available at: <http://dods.extra.cea.fr/data/p529viov/cruncep/readme.htm> (last access: December 2013), 2013.
- Viovy, N. and de Noblet, N.: Coupling water and Carbon cycle in the biosphere, *Sci. Géol. Bull.*, 50, 109–121, 1997.
- Vuichard, N., Ciais, P., Viovy, N., Calanca, P., and Soussana, J.-F.: Estimating the greenhouse gas fluxes of European grasslands with a process-based model: 2. Simulations at the continental level, *Global Biogeochem. Cy.*, 21, GB1005, doi:10.1029/2005GB002612, 2007a.
- Vuichard, N., Soussana, J.-F., Ciais, P., Viovy, N., Ammann, C., Calanca, P., Clifton-Brown, J., Fuhrer, J., Jones, M., and Martin, C.: Estimating the greenhouse gas fluxes of European grasslands with a process-based model: 1. Model evaluation from in situ measurements, *Global Biogeochem. Cy.*, 21, G01002, doi:10.1029/2004JG000004, 2007b.
- Wang, T., Ottlé, C., Boone, A., Ciais, P., Brun, E., Morin, S., Krinner, G., Piao, S., and Peng, S.: Evaluation of an improved intermediate complexity snow scheme in the ORCHIDEE land surface model, *J. Geophys. Res.-Atmos.*, 118, 6064–6079, 2013.
- Warneck, P., *Chemistry of the Natural Atmosphere*, 757 pp., Academic, San Diego, Calif., 1988.
- Zeng, C., Wu, J., and Zhang, X.: Effects of grazing on above- vs. below-ground biomass allocation of alpine grasslands on the northern Tibetan Plateau, *PLoS ONE*, 10, e0135173, doi:10.1371/journal.pone.0135173, 2015.
- Zhang, Y., Yu, Q., Jiang, J., and Tang, Y.: Calibration of Terra/MODIS gross primary production over an irrigated cropland on the North China Plain and an alpine meadow on the Tibetan Plateau, *Glob. Change. Biol.*, 14, 757–767, 2008.
- Zhao, M. and Running, S. W.: Drought-induced reduction in global terrestrial net primary production from 2000 through 2009, *Science*, 329, 940–943, 2010.
- Zhao, M., Heinsch, F. A., Nemani, R. R., and Running, S. W.: Improvements of the MODIS terrestrial gross and net primary production global data set, *Remote Sens. Environ.*, 95, 164–176, 2005.
- WorldClim: Global Climate Data, available at: <http://www.worldclim.org/>, last access: December 2014.